The Canadian Mineralogist
Vol. 57, pp. 605-635 (2019)
DOI: 10.3749/canmin.1900001

RELATIVE HUMIDITY AS A DRIVER OF STRUCTURAL CHANGE IN THREE NEW FERRIC-SULFATE-TELLURITE HYDRATES: NEW MINERALS TAMBOITE AND METATAMBOITE, AND A LOWER-HYDRATE DERIVATIVE, POSSIBLY INVOLVING DIRECT UPTAKE OF ATMOSPHERIC $\{H_2O\}_4$ CLUSTERS

Mark A. COOPER, Frank C. HAWTHORNE[§], and Yassir A. ABDU*

Department of Geological Sciences, University of Manitoba, Winnipeg, Manitoba, R3T 2N2, Canada

Phillip C. WALFORD

Marathon Gold Corporation, 10 King Street East, Suite 501, Toronto, Ontario M5C 1C3, Canada

Malcolm E. BACK

Department of Natural History (Mineralogy), Royal Ontario Museum, 100 Queen's Park, Toronto, Ontario, M5S 2C6, Canada

Abstract

Tamboite ($x = 3$; $y = 2$) and metatamboite ($x = 3$; $y = 0$), $Fe^{3+}{}_3(SO_4)(Te^{4+}O_3)_3(Te^{4+}O(OH)_2)(OH)(H_2O)_x\{H_2O\}_y$, are new tellurite minerals from the Tambo mine, Coquimbo Province, Chile. The two minerals transform to each other reversibly with changes in ambient humidity. They occur as pale-yellow clusters of radiating fiber bundles on the surface of a compact aggregate of silicified tuff. Tamboite and metatamboite are optically biaxial, and their calculated mean index of refraction is greater than 1.80. The calculated densities are 3.648 g/cm^3 for tamboite and 4.053 g/cm^3 for metatamboite. Tamboite and metatamboite are monoclinic, space group $P2_1/c$, $Z = 4$. Unit-cell parameters for tamboite are a 16.879(10), b 7.310(4), c 16.666(9) Å, β 108.857(11)°, V 1958(3) Å^3; for metatamboite they are a 14.395(5), b 7.296(4), c 16.411(6) Å, β 98.909(10)°, V 1703(2) Å^3. Chemical analysis by electron microprobe gave the empirical cations [calculated on the basis of 22 anions *pfu* with OH = 3 and H_2O = 5 *pfu* (tamboite) or H_2O = 3 *pfu* (metatamboite)] as $(Fe^{3+}{}_{3.10}Al_{0.15})_{\Sigma 3.25}(S^{6+}{}_{0.75}Se^{6+}{}_{0.05})_{\Sigma 0.80}Te^{4+}{}_{4.11}$. The seven strongest lines in the X-ray powder diffraction patterns [listed as d (Å), I, (hkl)] are as follows: metatamboite: 14.221, 100, (100); 2.874, 13, ($\bar{2}23$); 3.140, 12, (221); 3.423, 11, (121, $\bar{3}13$); 3.400, 11, (312); 3.012, 11, (313, $\bar{1}23$); 4.054, 9, ($\bar{1}04$, 004); tamboite: 16.068, 100, (100); 3.425, 9, (312, 212, $\bar{4}04$, 213); 2.999, 8, ($\bar{2}23$); 3.171, 6, (221); 2.853, 5, ($\bar{3}23$); 4.153, 4, ($\bar{1}04$); 3.943, 4, (004).

The crystal structures were solved by direct methods and refined to R_1 indices of 4.3 and 3.0%. The structures consist of virtually identical ferric-sulfate-tellurite-hydrate slabs that are constructed from strands of ferric-sulfate-hydrate polyhedra linked by Te^{4+} cations. In metatamboite, the slabs are linked directly by hydrogen bonds whereas in tamboite, interslab linkage occurs by hydrogen bonds through interstitial $\{H_2O\}_4$ clusters known as C_i cyclic tetramers. Exposure of a crystal to a desiccant at room temperature resulted in a third variant ($x = 2$; $y = 0$) with the structural formula $Fe^{3+}{}_2Fe^{2+}(SO_3(OH))(Te^{4+}O_3)_3(Te^{4+}O(OH)_2)(OH)(H_2O)_x$, space group $P2_1/c$, $Z = 4$, a 16.879(10), b 7.310(4), c 16.666(9) Å, β 108.857(11)°, V 1958(3) Å^3, calculated density 4.176 g/cm^3. This lower-hydrate variant has less cation-bonded (H_2O) than metatamboite and tamboite, and the ferric-sulfate-tellurite-hydrate slabs are polymerized to form a framework structure. Attempts to transform the lower hydrate back to tamboite or metatamboite at room temperature and elevated humidity were unsuccessful.

Keywords: tamboite, metatamboite, new mineral species, tellurite, Tambo mine, Coquimbo Province, Chile, crystal structure, electron-microprobe analysis, water clusters, C_i cyclic tetramers.

§ *Corresponding author email address*: frank_hawthorne@umanitoba.ca
* *Current address*: Department of Applied Physics and Astronomy, University of Sharjah, P.O. Box 27272, Sharjah, United Arab Emirates

Downloaded from https://pubs.geoscienceworld.org/canmin/article-pdf/57/5/605/4851376/i1499-1276-57-5-605.pdf
by University of Arizona user

Introduction

As part of our general interest in Se- and Te-oxysalt minerals (Back *et al*. 1999, 2017, Burns *et al*. 1995, Cooper & Hawthorne 1996, Cooper *et al*. 2008, Hawthorne 1984, Hawthorne *et al*. 1986, 1987, 2009, Tait *et al*. 2014), we describe two new mineral species from the Tambo mine, Chile. The amount of H_2O in these two minerals is dependent on the ambient humidity, and exposure of these minerals to a very low humidity in a sealed tube containing a strong desiccant led to the formation of a third phase, the crystal structure of which is also reported here. The new minerals and mineral names were approved by the Commission on New Minerals and Mineral Names, International Mineralogical Association (IMA 2016-059 and 2016-060). The minerals are named tamboite and metatamboite after the Tambo mine, Coquimbo Province, Chile. The holotype is deposited in the mineral collection of the Royal Ontario Museum, catalogue number M57171.

There has recently been a surge of activity in work on Te-oxysalt minerals, driven in part by the description and structural characterization of many new species (*e.g*., Kampf *et al*. 2010, 2013a, 2013b, 2016, 2017, 2018, Christy *et al*. 2015, Mills *et al*. 2014, Missen *et al*. 2018). In particular, Christy *et al*. (2016a) have produced an excellent analysis of the structural architecture of tellurium oxycompounds that provides a framework for future work on the paragenesis of these minerals. Following on from this, Christy *et al*. (2016b) analyzed the relationships between crystal structure, mineral composition, and paragenesis for secondary Te mineralization at the Bird Nest drift, Otto Mountain, California, producing major insights into the processes giving rise to the observed parageneses.

Occurrence

Tamboite and metatamboite were discovered by one of the authors (PCW) at the Wendy open pit, Tambo mine, El Indio-Tambo mining property, Coquimbo Province, Chile. The El Indio-Tambo mining property covers 1295 square kilometers of the El Indio Belt, a prolific gold, silver, and copper district located in Coquimbo Province, Chile, close to the border with Argentina in the Andes Mountains (approx. 70° W longitude and 30° S latitude). The property consists of two mines, the El Indio mine, a porphyry copper gold deposit, and the Tambo mine, located within five kilometers of each other in the south-central part of the property, and is at an elevation of approximately 3950 m. The mineralization in the Tambo area is characterized by high level epithermal veins and breccias located along approximately east–west structures. The Wendy open pit is one of three pits that have been worked at the Tambo mine. All the mining operations are now closed and the site has been reclaimed.

The regional and local geology of the area was described by Siddeley & Araneda (1986). These deposits are located in rhyolitic and dacitic pyroclastic volcanic rocks of Tertiary age (8–11 Ma) that are strongly hydrothermally altered. The Wendy pit is located on the south flank of Cerro Elefante, which is a north–south elongate accumulation of dacite tuffs. Hydrothermal breccias are a common feature of the Tambo mine and consist of silicified clasts of dacitic tuffs cemented by silica, baryte, and alunite (Siddeley & Araneda 1986). Tamboite and metatamboite, along with other tellurite minerals, occur in the interstices of the silicified hydrothermal breccias. Of the new tellurite minerals described from this locality [walfordite (Fe^{3+},Te^{6+},Ti^{4+},Mg)$Te^{4+}{}_3O_8$ and telluromandarinoite $Fe^{3+}{}_2Te^{4+}{}_3O_9(H_2O)_6$; Back *et al*. 1999, 2017], tamboite and metatamboite are by far the more common species.

Associated minerals are alunite, rodalquilarite, emmonsite, poughite, and mackayite; other minerals identified in the same matrix include scorodite, paratellurite, tellurite, baryte, gold, and native tellurium. Due to the extreme level of hydrothermal alteration, it is difficult to know the exact origin of the minerals. However, native tellurium, calaverite, krennerite, and other unidentified gold tellurides have been identified in the barite-alunite ores.

Physical Properties

Tamboite and metatamboite have very similar physical properties and are visually indistinguishable. Indeed, we observed the transition of a crystal of metatamboite to tamboite (in summer; lab $T = 21$ °C; relative humidity ~50%) and from tamboite to metatamboite (in winter; lab $T = 21$ °C; relative humidity <20%); this change is completely reversible at room temperature in response to changes in relative humidity. Both minerals are pale yellow with a very pale-yellow to colorless streak, greasy to vitreous, semi-translucent, and do not fluoresce in ultraviolet light. Crystal clusters (up to 3 mm across) of radiating fiber bundles (up to 1 mm long) (Fig. 1) occur on the surface of a compact aggregate of silicified tuff. The fiber bundles are flattened and commonly broaden from the base to reach a maximum width approximately one-third to one-half along their length and then narrow to become acicular toward the outer ends of the bundles (Fig. 2). The fiber bundles twist and merge near their ends, forming simple prisms flattened

Downloaded from https://pubs.geoscienceworld.org/canmin/article-pdf/57/5/605/4851376/i1499-1276-57-5-605.pdf
by University of Arizona user

FIG. 1. Radiating clusters of yellow tamboite–metatamboite fiber bundles decorating the surface of a silicified tuff.

on (100) and elongated along [010] and with terminal [possibly (012)] crystal faces (Fig. 3). The flattened terminal prism has uniform crisp optical extinction under the polarizing microscope and gives a simple X-ray diffraction pattern. We were not able to assess hardness or observe cleavage due to the fibrous nature of the material. Both minerals are brittle with a splintery fracture. The intimate fibrous character of the mineral precluded measurement of density; the calculated densities are 3.648 g/cm^3 for tamboite and 4.053 g/cm^3 for metatamboite.

Tamboite and metatamboite are optically biaxial, and the average indices of refraction calculated using the Gladstone-Dale relation are 1.874 for tamboite and 1.958 for metatamboite. Individual crystals are pleochroic colorless to very pale yellow, and fiber bundles become grey to greyish black in plane-polarized light.

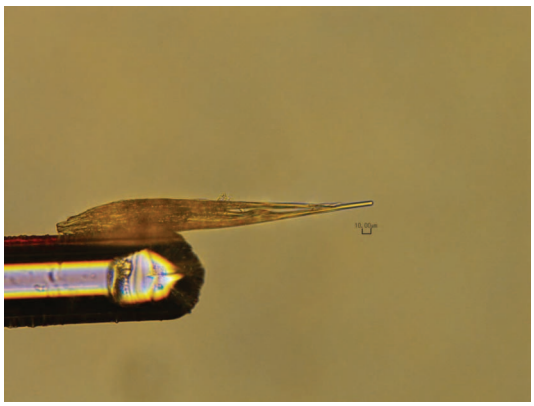

FIG. 2. A fiber bundle of tamboite–metatamboite containing a terminal prism glued to a glass fiber.

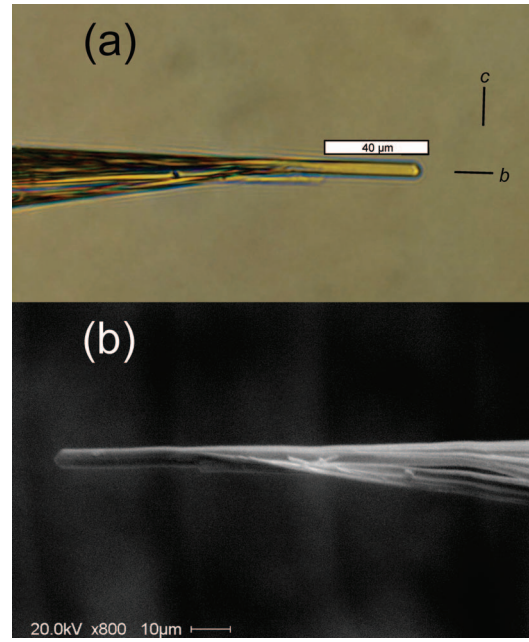

FIG. 3. A twisted assemblage of tamboite/metatamboite coalescing into a single crystal prism tip viewed onto (100): (a) under plane polarized light; (b) SEM-BSE image.

CHEMICAL COMPOSITION

A fiber bundle was polished and analyzed with a Cameca SX-100 electron microprobe operating in wavelength-dispersion mode with an accelerating voltage of 15 kV, a specimen current of 20 nA, and a beam diameter of 2 µm. The following standards were used: $FeTe_2O_6$ (Te), fayalite (Fe), andalusite (Al), stibnite (S), and synthetic CdSe (Se). The data were reduced and corrected by the PAP method of Pouchou & Pichoir (1985). Exposure to a high vacuum during application of the carbon coat and within the electron-microprobe most certainly affected the mineral with respect to its H_2O content, and the exact nature of the material exposed to the electron beam remains unknown. Additionally, because the mineral occurs as a finely twisted crystal composite, single flat surfaces were not available for analysis. Table 1 gives the chemical composition (mean of two determinations) and establishes a simple ~4:3:1 stoichiometry for Te^{4+}:Fe^{3+}:S^{6+} in tamboite and metatamboite. The empirical formula unit calculated for tamboite ($x = 3$; $y = 2$) and metatamboite ($x = 3$; $y = 0$), where x and y

Downloaded from https://pubs.geoscienceworld.org/canmin/article-pdf/57/5/605/4851376/i1499-1276-57-5-605.pdf
by University of Arizona user

TABLE 1. CHEMICAL DATA FOR TAMBOITE, METATAMBOITE, LOWER HYDRATE

	Tamboite $Fe^{3+}{}_3(SO_4)(Te^{4+}O_3)_3(Te^{4+}O(OH)_2)(OH)(H_2O)_3\{H_2O\}_2$	Metatamboite $Fe^{3+}{}_3(SO_4)(Te^{4+}O_3)_3(Te^{4+}O(OH)_2)(OH)(H_2O)_3$	Lower hydrate (LH) $Fe^{3+}{}_2Fe^{2+}(SO_3(OH))(Te^{4+}O_3)_3(Te^{4+}O(OH)_2)(OH)(H_2O)_2$
Bonded (H_2O) *pfu*	3	3	2
Interstitial $\{H_2O\}$ *pfu*	2	0	0
wt.% oxide*			
TeO_2	63.90	63.90	63.90
Fe_2O_3††	24.14	24.14	16.36
FeO††	–	–	7.00
Al_2O_3	0.75	0.75	0.75
SO_3	5.84	5.84	5.84
SeO_3	0.63	0.63	0.63
H_2O†	11.41	7.90	7.02
Total	106.67	103.16	101.50
Anions *pfu*†			
O^{2-}	14	14	14
$(OH)^-$	3	3	4
(H_2O)	5	3	2
Anion Total	22	20	19
Ideal wt.% oxide			
TeO_2	59.38	61.45	62.47
Fe_2O_3††	22.28	23.05	15.62
FeO††	–	–	7.03
SO_3	7.45	7.70	7.83
H_2O†	10.89	7.80	7.05
Total	100.00	100.00	100.00

* Mean of two determinations; † calculated from structure; †† Fe^{2+}/Fe^{3+} partitioning for LH from structure.

refer to cation-bonded and interstitial H_2O groups, respectively, is $(Fe^{3+}{}_{3.10}Al_{0.15})_{\Sigma 3.25}(S^{6+}{}_{0.75}Se^{6+}{}_{0.05})_{\Sigma 0.80}Te^{4+}{}_{4.11}O_{14}(OH)_3(H_2O)_{x+y}$. The simplified general formula for tamboite ($x = 3$; $y = 2$) and metatamboite ($x = 3$; $y = 0$) is $Fe^{3+}{}_3(SO_4)(Te^{4+}O_3)_3(Te^{4+}O(OH)_2)(OH)(H_2O)_x\{H_2O\}_y$. Highlighting the distinction between the two types of H_2O within the formula unit is paramount to the understanding the relations between tamboite, metatamboite, and the lower hydrate (*i.e.*, with less H_2O in the structure).

Infrared Spectroscopy

The FTIR spectrum of tamboite–metatamboite (Fig. 4) was collected on a thin film, prepared with a Diamond Micro Compression Cell, using a Bruker Hyperion 2000 IR microscope equipped with a liquid-nitrogen-cooled MCT detector. Data over the range 4000–650 cm^{-1} were obtained by averaging 100 scans with a resolution of 4 cm^{-1}. A strong and broad band centered at ~3200 cm^{-1} and a sharp peak at 1638 cm^{-1} (with a shoulder at 1610 cm^{-1}) are due to H_2O stretches and H–O–H bends, respectively, and indicate the presence of a considerable amount of H_2O in tamboite–metatamboite. Shoulders located on the high-frequency side of the broad band, particularly at ~3420 and 3500 cm^{-1}, are indicative of the presence of OH groups in the tamboite–metatamboite structure. Strong to medium intensity peaks in the 1300–900 cm^{-1} region (1202, 1142, 1105, 1055, 1031, and 988 cm^{-1}) are assigned to S–O stretching vibrations and peaks below 800 cm^{-1} (772, 745, 714, and 667 cm^{-1}) are assigned to Te–O stretches.

X-Ray Diffraction

Tamboite and metatamboite are visually identical and can be reliably distinguished only by their very different unit-cell parameters. We have characterized the fully ordered structural arrangements for both minerals occurring at ambient temperature and different relative humidities.

Each fiber bundle broadens strongly from the base, where it attaches to the matrix, reaches a maximum

Downloaded from https://pubs.geoscienceworld.org/canmin/article-pdf/57/5/605/4851376/i1499-1276-57-5-605.pdf
by University of Arizona user

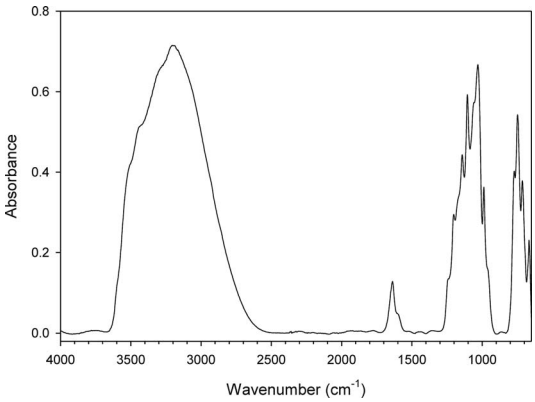

FIG. 4. The infrared spectrum for tamboite–metatamboite.

diameter 1/4 to 1/3 along the length of the bundle, and then narrows progressively toward the tip of the fiber, where a single crystal is formed approximately 3–4 μm wide and typically <100 μm long (Fig. 2). Close to the tip, the fibers twist and coalesce into a single crystal (Fig. 3). We received the tamboite/metatamboite sample from the Royal Ontario Museum in winter (February 2015) and mounted a crystal (crystal #1). An entire fiber bundle (as in Fig. 2) was attached to a glass fiber, with only the crystal tip centered in the X-ray beam; X-ray intensity data were collected and the structure of metatamboite was solved and refined. This X-ray crystal (crystal #1) was re-examined approximately six months later in the summer (August 2015) and gave different unit-cell parameters on the diffractometer. We then tested a second crystal (crystal #2) taken from the rock sample, which also gave this same new unit cell. We collected X-ray intensity data (crystal #2) and then solved and refined the crystal structure of tamboite. This tamboite crystal (crystal #2) was left exposed to air to be re-examined the following winter. Our previous metatamboite crystal from February 2015 (crystal #1), which had spontaneously hydrated to tamboite (August 2015), was then moved to an artificial low-humidity environment in August 2015 by sealing it in a test tube containing silica-gel desiccant beads; it was then re-examined in the winter (January 2016). Upon aligning this crystal (crystal #1) on the X-ray diffractometer, the tip was observed to be bent by curvature of the {100} faces about a direction normal to the fiber length (Fig. 5), and the diffraction pattern contained markedly streaked diffraction spots consistent with a bent crystal. Additionally, the crystal tip appeared darker in color (brown). Nevertheless, a unit-cell could be extracted from preliminary data frames on this bent crystal (crystal #1), and it was different from the unit

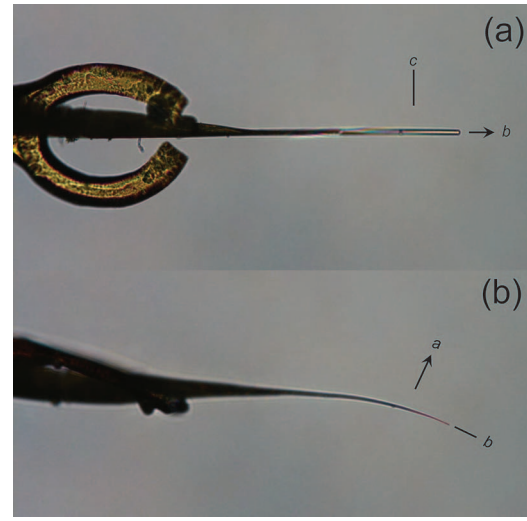

FIG. 5. A fiber-tip crystal of the lower hydrate LH mounted on a polymer loop and viewed under a binocular microscope: (a) onto (100), (b) down [001].

cells of both metatamboite (February 2015) and tamboite (August 2015) that were measured from the same crystal. An X-ray intensity data set was collected from this bent crystal (crystal #1) and structure solution revealed a third structural variant with an even lower hydration state (herein referred to as LH for lower hydrate). The tamboite crystal (crystal #2) from August 2015 (higher humidity) that had been left exposed to the air was re-measured in January 2016 (lower humidity) and found to correspond to the metatamboite unit-cell. Thus, conversion from metatamboite to tamboite (and the reverse) occurs at room temperature (21 °C), where the seasonally dependent relative humidity dictates which particular hydrate is present (*i.e.*, tamboite in summer and metatamboite in winter). However, the bent LH crystal (crystal #1) retained both its bent shape and unit cell through the following summer and winter, indicating that rehydration and conversion back to tamboite or metatamboite does not occur at room temperature and higher humidity.

X-ray powder diffraction

In a later section, we discuss the strong probability that individual fiber bundles consist of both tamboite and metatamboite, and hence the X-ray powder diffraction data presented for tamboite and metatamboite (Fig. 6) were calculated using single-crystal X-ray diffraction intensities from the pure phases. The (100) reflection was experimentally obscured behind the beam stop; it is included in Table 2 as the 100%

Downloaded from https://pubs.geoscienceworld.org/canmin/article-pdf/57/5/605/4851376/i1499-1276-57-5-605.pdf
by University of Arizona user

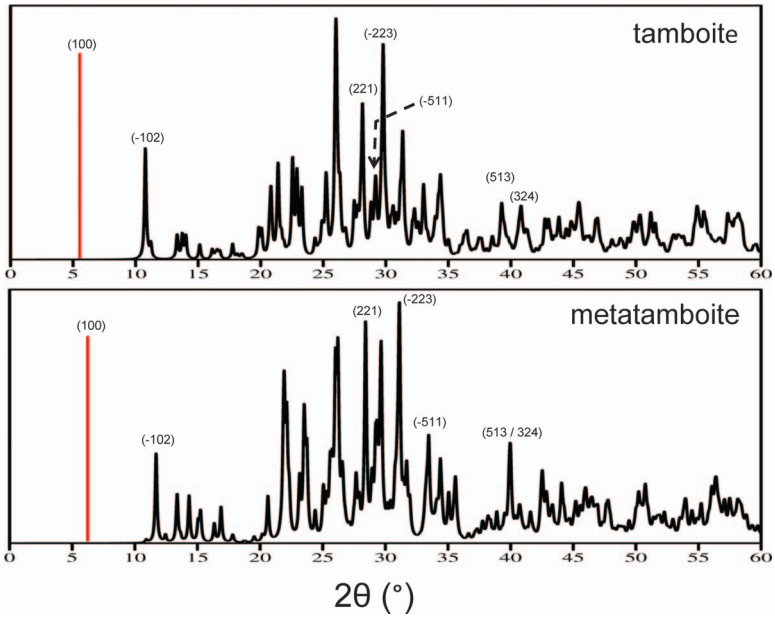

FIG. 6. Powder X-ray diffraction data for tamboite and metatamboite generated from single-crystal X-ray intensities (λ = 1.54178 Å).

relative *I* peak based on its intensity calculated from the structure arrangement. All observed intensities have been scaled relative to the unobserved (100) intensity in Table 2; note that the (100) reflection intensity is very strong relative to the rest of the pattern and that the detail in the rest of the pattern has been visually enhanced in Figure 6 by scaling it to the full vertical range and then inserting the unscaled (100) peak as a simple marker position (red line in each figure). We anticipate very significant preferred orientation effects to occur in an experimental smear mount, with the bladed (100) morphology likely rendering a near-featureless diffraction pattern above 10° 2θ. A few simple peaks have their indices labelled for visual comparison between the two patterns (Fig. 6). Both minerals contain significant H, which could not be reliably located in the difference-Fourier maps and is therefore absent in the structure-refinement models; the practice of presenting simulated powder data in terms of the actual observed single-crystal intensities is important in this regard as being representative, rather than using the intensities calculated from the (H deficient) structure-refinement model.

Single-crystal diffraction

An entire fiber bundle was attached to a glass fiber or polymer loop (*e.g.*, Figs. 2 and 5) and mounted on a Bruker D8 three-circle diffractometer equipped with a rotating-anode generator (Mo*K*α), multilayer optics, and an APEX II 4K CCD detector. The flattened prism tip was centered in the X-ray beam (~120 μm beam diameter) and produced a simple single-crystal X-ray diffraction pattern. The entire Ewald sphere of intensities (including additional redundant reflections) was collected with a crystal-to-detector distance of 5 cm (Table 3). Empirical absorption corrections (SADABS, Sheldrick 2008) were applied and equivalent reflections merged. All calculations were done with the SHELXTL PC (Plus) system of programs; *R* indices are of the form given in Table 3 and are expressed as percentages. Systematic absences in the single-crystal X-ray diffraction data are consistent with space group $P2_1/c$, and the structure was solved with this symmetry by direct methods and refined by full-matrix least-squares. Atom positions and displacement parameters are given in Table 4, selected interatomic distances are given in Table 5, and bond valences are given in Tables 6 and 7.

Downloaded from https://pubs.geoscienceworld.org/canmin/article-pdf/57/5/605/4851376/i1499-1276-57-5-605.pdf
by University of Arizona user

TABLE 2. POWDER X-RAY DIFFRACTION DATA GENERATED FROM SINGLE-CRYSTAL X-RAY DIFFRACTION DATA FOR METATAMBOITE AND TAMBOITE

Metatamboite			Tamboite		
I (%)	*d* (Å)	*h k l*	*I* (%)	*d* (Å)	*h k l*
100*	14.221	100	100*	16.068	100
5	7.565	$\bar{1}02$	4	8.205	$\bar{1}02$
1	7.111	200	1	7.889	002
3	6.617	102	1	6.645	110 / 011
3	6.179	$\bar{1}11$	1	6.447	$\bar{1}11$
1	5.881	111	1	6.318	102
2	5.812	$\bar{2}02$	1	5.856	111
1	5.423	012	1	4.994	$\bar{2}12$
2	5.252	$\bar{1}12$	1	4.474	$\bar{3}11$
1	4.398	$\bar{3}02$	1	4.424	$\bar{1}13$
3	4.306	$\bar{1}13$	3	4.267	013 $\bar{2}13$
9	4.054	$\bar{1}04$ / 004	4	4.153	$\bar{1}04$
8	4.017	113	1	4.107	$\bar{2}04$
4	3.840	302	1	4.070	212
7	3.781	$\bar{2}04$	1	4.012	400
6	3.750	104	4	3.943	004
2	3.648	020	3	3.884	302 / 113
3	3.553	400 / $\bar{1}14$	3	3.819	$\bar{3}04$
3	3.516	213	1	3.655	020
5	3.479	$\bar{1}21$	1	3.574	$\bar{2}14$
5	3.459	$\bar{4}02$	3	3.530	$\bar{1}21$ / 410
11	3.423	121 / $\bar{3}13$	9	3.425	312 / 212 / $\bar{4}04$ / 213
11	3.400	312	3	3.386	$\bar{3}14$ / $\bar{5}02$
4	3.357	$\bar{2}14$ / $\bar{3}04$	1	3.331	220
1	3.287	$\bar{1}22$	2	3.245	411
4	3.224	$\bar{2}21$ / $\bar{4}11$	2	3.213	500
3	3.197	410	6	3.171	221
12	3.140	221	2	3.097	$\bar{4}14$
4	3.085	$\bar{2}22$ / 402	3	3.059	$\bar{5}11$
6	3.053	411	8	2.999	$\bar{2}23$
7	3.044	$\bar{3}14$	2	2.937	$\bar{3}15$
11	3.012	313 / $\bar{1}23$	2	2.922	412
2	2.963	015	2	2.896	015
2	2.938	222 / $\bar{4}13$	5	2.853	$\bar{3}23$
13	2.874	$\bar{2}23$	2	2.772	$\bar{4}15$
4	2.843	500 / 412	1	2.748	511
4	2.823	115	3	2.713	115
3	2.802	321	1	2.639	$\bar{3}24$ / $\bar{6}12$
6	2.678	$\bar{5}11$	3	2.609	$\bar{6}11$
2	2.626	$\bar{2}24$	1	2.563	$\bar{1}16$ / $\bar{3}16$
5	2.607	215	1	2.497	215
3	2.560	$\bar{1}16$ / $\bar{4}21$	1	2.476	$\bar{5}21$
4	2.522	$\bar{3}06$	1	2.463	$\bar{5}06$
1	2.409	$\bar{4}23$	1	2.401	422
1	2.382	$\bar{3}16$	1	2.390	224 / 025
1	2.355	422	1	2.337	$\bar{1}32$
1	2.346	125	2	2.294	513
2	2.315	$\bar{1}32$	1	2.267	$\bar{7}11$
2	2.279	$\bar{6}11$	1	2.255	$\bar{3}17$
5	2.256	$\bar{5}21$ / 324 / 513	2	2.211	324
2	2.232	$\bar{1}17$	1	2.190	$\bar{1}26$

Downloaded from https://pubs.geoscienceworld.org/canmin/article-pdf/57/5/605/4851376/i1499-1276-57-5-605.pdf
by University of Arizona user

TABLE 2. CONTINUED.

Metatamboite			Tamboite		
I (%)	*d* (Å)	*h k l*	*I* (%)	*d* (Å)	*h k l*
2	2.216	225	1	2.116	$\bar{5}17$
2	2.171	026	1	2.103	$\bar{4}32$ / $\bar{1}34$
4	2.126	$\bar{3}32$ / $\bar{3}17$	1	2.065	332
3	2.110	316	1	2.039	$\bar{1}08$
2	2.088	$\bar{1}34$	1	2.022	316
1	2.075	$\bar{3}26$	2	1.996	$\bar{2}18$ / $\bar{7}21$ / $\bar{2}27$
3	2.055	332	1	1.971	$\bar{7}24$
1	2.033	$\bar{2}08$	1	1.962	$\bar{1}18$
1	2.027	008	1	1.941	$\bar{8}15$
2	2.006	406 / $\bar{6}21$	1	1.937	810 / 432
2	1.991	$\bar{6}22$	1	1.892	$\bar{5}27$
3	1.973	$\bar{1}18$ / $\bar{1}27$	1	1.868	721 / 416
2	1.953	018	1	1.846	$\bar{6}32$
2	1.942	621	1	1.830	$\bar{2}36$ / 040
2	1.936	416	2	1.813	140 / $\bar{6}27$ / 802
1	1.920	604	1	1.785	900 / $\bar{4}36$ / $\bar{2}19$ / $\bar{4}19$
2	1.904	135 / 702	1	1.773	$\bar{9}15$
1	1.884	$\bar{6}24$	1	1.753	704
1	1.873	$\bar{6}16$	1	1.727	043
1	1.865	$\bar{4}34$	1	1.717	$\bar{7}32$ / 533
1	1.857	614	1	1.704	714 / 019
1	1.843	$\bar{5}32$	2	1.673	$\bar{4}42$ / $\bar{1}44$
3	1.816	$\bar{1}36$ / $\bar{4}27$	2	1.658	044
2	1.810	140	2	1.607	$\bar{5}42$ / 10,00
3	1.799	$\bar{7}15$	1	1.601	633
1	1.777	$\bar{4}35$ / 800	2	1.592	336
2	1.762	$\bar{2}19$	2	1.585	$\bar{6}37$
2	1.750	$\bar{3}36$	1	1.555	541
1	1.729	128 / 043	1	1.551	921
1	1.712	704 / 242			
2	1.699	$\bar{6}32$ / 533			
2	1.684	$\bar{3}42$			
1	1.673	$\bar{6}08$			
2	1.663	044			
3	1.640	144			
4	1.632	336 / 517 / $\bar{1}29$			
2	1.614	$\bar{4}42$			
2	1.603	$\bar{5}36$			
2	1.586	$\bar{4}37$			
1	1.570	633			
1	1.559	730			
1	1.548	436			

* Unobserved experimentally and inserted on a relative scale.

Crystal Structure

General structural details pertaining to tamboite and metatamboite will be discussed in parallel, as these two structures are very similar and differ primarily in terms of interstitial $\{H_2O\}$ content. Structural investigation of the completely reversible transition between tamboite and metatamboite is of particular interest, considering that both atomic arrangements have been well determined and potentially hold clues to the hydration $\leftrightarrow$ dehydration mechanism. The lower hydrate (LH) structure contains a fundamental difference in connectivity, as the structural units are polymerized relative to the isolated

Downloaded from https://pubs.geoscienceworld.org/canmin/article-pdf/57/5/605/4851376/i1499-1276-57-5-605.pdf
by University of Arizona user

TABLE 3. MISCELLANEOUS INFORMATION FOR TAMBOITE, METATAMBOITE, AND LOWER HYDRATE

	Tamboite $Fe^{3+}{}_3(SO_4)(Te^{4+}O_3)_3(Te^{4+}O(OH)_2)(OH)(H_2O)_3\{H_2O\}_2$	Metatamboite $Fe^{3+}{}_3(SO_4)(Te^{4+}O_3)_3(Te^{4+}O(OH)_2)(OH)(H_2O)_3$	Lower hydrate [LH] $Fe^{3+}{}_2Fe^{2+}(SO_3(OH))(Te^{4+}O_3)_3(Te^{4+}O(OH)_2)(OH)(H_2O)_2$
Crystal	#2	#1	#1
Z	4	4	4
a (Å)	16.979(10)	14.395(5)	14.50(2)
b	7.310(4)	7.296(4)	7.326(11)
c	16.666(9)	16.411(6)	16.41(2)
β (°)	108.857(11)	98.909(10)	111.18(2)
V (Å^3)	1958(3)	1703(2)	1625(7)
a:*b*:*c*	2.3227:1:2.2799	1.9730:1:2.2493	1.9793:1:2.2400
Space group	$P2_1/c$	$P2_1/c$	$P2_1/c$
Unit cell reflections	$4088 > 8\sigma I$	$4062 > 8\sigma I$	$2845 > 5\sigma I$
Total reflections	45543	41023	17673
Ewald reflections	12873	11540	8277
Unique reflections	3435	3020	2118
No. with $F_o > 4\sigma F$	2954	2461	1093
R_{merge} %	5.0	5.2	31.5
R_1 %	4.3	3.0	25.4
wR_2 %	10.3	7.3	49.1
A, B weights	0.0312, 52.70	0.0343, 8.30	0.2, 0
Crystal size* (μm)	~3 × 10	~2 × 8	~2 × 8
Frame time (s)	160	78	180
Frame width (°)	0.5	0.3	0.5
2θ limit (°)	50	50	45
D_{calc} (g/cm^3)	3.648	4.053	4.176
Mean R.I.$_{calc}$	1.874	1.958	1.943

* Thickness × width; ~120 μm of the crystal along its length was exposed to the X-ray beam.
$R_1 = \Sigma(|FO| - |Fc|) / \Sigma|Fc$
$wR_2 = [\Sigma w(F^2o - F^2c)^2 / \Sigma w(F^2o)^2]^{1/2}$,
$w = 1 / [\sigma^2(F^2o) + (A\ P)^2 + B\ P]$ where $P = (\max(F^2o,0) + 2F^2c) / 3$

units in tamboite and metatamboite. Details pertaining to the (LH) structure will follow in a later section.

Cation site-occupancies

The cation sites (excluding H) in tamboite and metatamboite are the same and a single description is sufficient (Tables 4 and 5). Cation sites are indicated by italicized letters, *e.g.*, *Te*(1) and *Fe*(1), whereas specific cations are indicated by non-italicized letters, *e.g.*, Te(1) and Fe(1); polyhedra are denoted by the central cation, *e.g.*, Te(1) and Fe(1) polyhedra. There are four *Te* sites, occupied by Te^{4+}, with three short (~1.9 Å) bonds to O atoms on one side, forming a pyramid with Te^{4+} at the apex, a typical coordination for Te^{4+} with stereochemically active lone-pair electrons (Christy *et al.* 2016a, Gagné & Hawthorne 2018a). Additionally, there are from six to eight bonds from ~2.5 to 3.9 Å to more distant anions. Te(1), Te(2), and Te(3) each form three short bonds to O^{2-} ions, whereas Te(4) bonds to one O^{2-} ion and two $(OH)^-$ groups; we write these groups as $(Te^{4+}O_3)_3(Te^{4+}O(OH)_2)$ in the formula unit. There are three *Fe* sites, octahedrally coordinated by O^{2-} anions, $(OH)^-$ groups, and (H_2O) groups [$Fe(1)O_6$, $Fe(2)O_5(OH)$, $Fe(3)O_3(OH)(H_2O)_2$], with <Fe–Φ> distances (Φ indicates an unspecified anion) from 2.00 to 2.04 Å, indicating occupancy by Fe^{3+}. A single *S* site is tetrahedrally coordinated by four O^{2-} ions with a <*S*–O> distance of ~1.47 Å, typical of S^{6+} (Hawthorne *et al.* 2000, Gagné & Hawthorne 2018b).

Anion identity

In the tamboite and metatamboite structures, the anions O(1)–O(14) have incident bond-valence sums from 1.47 to 2.08 *vu* (without any contribution from H atoms) and are all O^{2-} ions (Tables 6 and 7). The OH(1), OH(2), and OH(3) anions have incident bond-valence sums from 1.11 to 1.19 *vu* (without any contribution from H atoms) and are OH groups: two

Downloaded from https://pubs.geoscienceworld.org/canmin/article-pdf/57/5/605/4851376/i1499-1276-57-5-605.pdf
by University of Arizona user

TABLE 4. ATOM COORDINATES AND DISPLACEMENT PARAMETERS (Å^2) FOR TAMBOITE, METATAMBOITE, AND LOWER HYDRATE

Site	x	y	z	U^{11}	U^{22}	U^{33}	U^{23}	U^{13}	U^{12}	U_{eq}/U_{iso}
Te(1)	0.10045(4)	0.11220(9)	0.50675(4)	0.0135(4)	0.0056(4)	0.0095(4)	0.0004(3)	0.0051(3)	0.0003(3)	0.00918(19)
	0.11405(3)	0.11119(7)	0.48810(3)	0.0165(3)	0.0056(3)	0.0094(3)	0.00035(19)	0.00096(19)	0.0004(2)	0.01061(14)
	0.1222(4)	0.1114(10)	0.5128(5)							0.0203(17)
Te(2)	0.81569(4)	0.10822(9)	–0.02662(4)	0.0129(1)	0.0065(4)	0.0101(4)	0.0004(3)	0.0055(3)	0.0005(3)	0.00942(19)
	0.79188(3)	0.10860(7)	0.00644(3)	0.0173(3)	0.0074(3)	0.0091(3)	0.0007(2)	0.00162(19)	0.0005(2)	0.01129(14)
	0.7787(4)	0.1116(10)	–0.0353(5)							0.0214(17)
Te(3)	0.00104(4)	0.13724(9)	0.71679(4)	0.0165(4)	0.0072(3)	0.0112(4)	0.0009(3)	0.0076(3)	0.0005(3)	0.01088(19)
	0.00124(4)	0.13559(7)	0.71525(3)	0.0209(3)	0.0082(3)	0.0102(3)	0.0008(2)	0.00259(19)	0.0006(2)	0.01308(14)
	0.0018(4)	0.1310(10)	0.7141(5)							0.0224(17)
Te(4)	0.21777(5)	0.08142(10)	0.27789(5)	0.0182(4)	0.0105(4)	0.0129(4)	–0.0009(3)	0.0060(3)	–0.0022(3)	0.0136(2)
	0.24343(4)	0.08050(8)	0.23946(3)	0.0216(3)	0.0115(3)	0.0115(3)	–0.0004(2)	0.0010(2)	–0.0023(2)	0.01504(15)
	0.2633(5)	0.0872(11)	0.2900(5)							0.0277(19)
Fe(1)	0.01378(9)	0.0020(2)	0.09581(9)	0.0125(8)	0.0070(7)	0.0075(7)	–0.0001(6)	0.0047(6)	0.0004(6)	0.0087(3)
	0.01513(7)	0.00184(16)	0.09342(6)	0.0178(5)	0.0065(6)	0.0060(5)	–0.0008(4)	0.0004(4)	0.0004(4)	0.0102(2)
	0.0190(9)	0.002(2)	0.0984(9)							0.017(3)
Fe(2)	0.87205(10)	0.3328(2)	0.81165(10)	0.0142(8)	0.0059(7)	0.0112(8)	0.0007(6)	0.0069(6)	–0.0005(6)	0.0098(3)
	0.85460(8)	0.33121(16)	0.83190(7)	0.0185(6)	0.0061(6)	0.0106(5)	0.0011(5)	0.0019(4)	–0.0006(5)	0.0117(3)
	0.8443(9)	0.329(2)	0.8014(10)							0.023(3)
Fe(3)	0.28760(10)	0.0204(2)	0.61902(10)	0.0108(8)	0.0083(8)	0.0154(8)	–0.0005(6)	0.0043(6)	–0.0011(6)	0.0115(3)
	0.32573(8)	0.02017(16)	0.57013(7)	0.0156(6)	0.0094(6)	0.0168(6)	0.0002(5)	–0.0002(4)	–0.0006(5)	0.0142(3)
	0.3439(9)	0.025(2)	0.6346(10)							0.017(3)
S	0.60670(18)	0.1753(4)	0.78153(19)	0.0158(15)	0.0121(14)	0.0213(15)	–0.0015(12)	0.0025(12)	–0.0002(11)	0.0173(6)
	0.55425(15)	0.1701(3)	0.85691(14)	0.0230(11)	0.0140(12)	0.0298(12)	–0.0057(9)	–0.0024(9)	–0.0011(9)	0.0230(5)
	0.529(2)	0.140(5)	0.811(2)							0.044(8)
O(1)	0.5286(6)	0.0864(13)	0.7761(6)	0.021(5)	0.024(5)	0.040(6)	–0.002(4)	0.005(4)	–0.002(4)	0.029(2)
O(1)	0.4741(6)	0.0769(12)	0.8771(7)	0.044(5)	0.038(5)	0.126(9)	0.000(6)	0.021(5)	–0.019(4)	0.069(3)
OH(4)	0.502(4)	–0.002(10)	0.877(5)							0.030(4)*
O(2)	0.6080(6)	0.2480(13)	0.6988(5)	0.033(5)	0.030(5)	0.015(4)	–0.001(4)	0.006(4)	0.004(4)	0.027(2)
	0.5445(5)	0.2186(13)	0.7688(4)	0.065(5)	0.070(6)	0.022(4)	–0.010(4)	–0.007(3)	0.044(5)	0.054(2)
	0.438(4)	0.167(10)	0.743(5)							0.030(4)*

Downloaded from https://pubs.geoscienceworld.org/canmin/article-pdf/57/5/605/4851376/i1499-1276-57-5-605.pdf
by University of Arizona user

TABLE 4. CONTINUED.

Site	x	y	z	U^{11}	U^{22}	U^{33}	U^{23}	U^{13}	U^{12}	U_{eq}/U_{iso}
O(3)	0.6772(5)	0.0454(11)	0.8138(5)	0.024(5)	0.017(4)	0.022(5)	0.004(4)	–0.001(4)	0.006(4)	0.0234(19)
	0.6409(5)	0.0599(9)	0.8769(4)	0.041(4)	0.015(3)	0.028(3)	–0.001(3)	–0.008(3)	0.010(3)	0.0294(15)
	0.621(4)	0.089(10)	0.796(5)							0.030(4)*
O(4)	0.6211(5)	0.3309(11)	0.8436(5)	0.019(4)	0.010(4)	0.025(5)	–0.004(3)	0.007(3)	–0.002(3)	0.0178(17)
	0.5672(4)	0.3437(9)	0.9042(4)	0.025(3)	0.020(4)	0.040(4)	–0.014(3)	0.007(3)	–0.003(3)	0.0282(15)
	0.545(4)	0.325(10)	0.847(5)							0.030(4)*
O(5)	0.2007(5)	0.2064(10)	0.5780(5)	0.016(4)	0.008(4)	0.013(4)	0.001(3)	–0.000(3)	–0.002(3)	0.0137(17)
	0.2278(4)	0.2042(8)	0.5423(3)	0.021(3)	0.008(3)	0.016(3)	–0.002(2)	–0.001(2)	–0.003(2)	0.0155(12)
	0.238(4)	0.196(10)	0.587(5)							0.030(4)*
O(6)	0.0646(5)	–0.0012(10)	0.5898(5)	0.016(4)	0.006(4)	0.027(4)	0.001(3)	0.014(3)	0.003(3)	0.0147(17)
	0.0739(4)	–0.0030(8)	0.5788(3)	0.016(3)	0.013(3)	0.015(3)	0.001(2)	0.002(2)	0.001(2)	0.0147(12)
	0.076(4)	–0.009(10)	0.588(5)							0.030(4)*
O(7)	0.0446(4)	0.3424(10)	0.5074(5)	0.010(4)	0.011(4)	0.010(4)	–0.000(3)	0.002(3)	0.001(3)	0.0106(15)
	0.0512(4)	0.3428(8)	0.4989(3)	0.020(3)	0.008(3)	0.011(3)	–0.000(2)	–0.000(2)	0.004(2)	0.0134(12)
	0.048(4)	0.327(10)	0.503(5)							0.030(4)*
O(8)	0.9091(5)	0.1362(11)	0.0694(5)	0.011(4)	0.025(5)	0.013(4)	0.002(3)	0.001(3)	0.006(3)	0.0170(17)
	0.8986(4)	0.1404(8)	0.0858(3)	0.022(3)	0.023(4)	0.008(3)	–0.005(2)	–0.002(2)	0.005(3)	0.0179(13)
	0.893(4)	0.130(10)	0.063(5)							0.030(4)*
O(9)	0.7914(5)	0.3598(10)	–0.0344(5)	0.020(4)	0.007(4)	0.016(4)	–0.000(3)	0.009(3)	0.001(3)	0.0134(16)
	0.7606(4)	0.3587(8)	0.0032(3)	0.018(3)	0.010(3)	0.016(3)	–0.000(2)	–0.004(2)	0.002(2)	0.0155(12)
	0.751(4)	0.378(10)	–0.042(5)							0.030(4)*
O(10)	0.8744(4)	0.1234(10)	–0.1100(5)	0.010(4)	0.010(4)	0.012(4)	–0.004(3)	0.005(3)	–0.002(3)	0.0106(15)
	0.8571(3)	0.1211(7)	–0.0881(3)	0.015(3)	0.008(3)	0.012(3)	0.003(2)	0.004(2)	0.002(2)	0.0115(11)
	0.848(4)	0.125(10)	–0.113(5)							0.030(4)*
O(11)	0.0993(5)	0.0045(10)	0.7651(5)	0.016(4)	0.005(4)	0.015(4)	–0.001(3)	0.008(3)	0.002(3)	0.0113(16)
	0.1110(4)	0.0060(8)	0.7493(3)	0.024(3)	0.008(3)	0.013(3)	–0.001(2)	0.003(2)	0.000(2)	0.0151(12)
	0.119(4)	0.006(10)	0.769(5)							0.030(4)*
O(12)	0.0575(5)	0.3536(10)	0.7021(4)	0.017(4)	0.016(4)	0.008(4)	0.001(3)	0.007(3)	–0.006(3)	0.0127(16)
	0.0646(4)	0.3518(8)	0.6918(3)	0.016(3)	0.010(3)	0.012(3)	0.001(2)	0.002(2)	–0.003(2)	0.0125(11)
	0.070(4)	0.346(10)	0.709(5)							0.030(4)*
O(13)	–0.0078(5)	0.2096(10)	0.8240(5)	0.013(4)	0.011(4)	0.012(4)	0.001(3)	0.004(3)	0.002(3)	0.0121(16)
	–0.0094(4)	0.2093(7)	0.8253(3)	0.020(3)	0.005(3)	0.007(2)	0.002(2)	0.002(2)	–0.001(2)	0.0109(11)
	–0.009(4)	0.201(10)	0.828(5)							0.030(4)*

Downloaded from https://pubs.geoscienceworld.org/canmin/article-pdf/57/5/605/4851376/i1499-1276-57-5-605.pdf
by University of Arizona user

TABLE 4. CONTINUED.

Site	x	y	z	U^{11}	U^{22}	U^{33}	U^{23}	U^{13}	U^{12}	U_{eq}/U_{iso}
O(14)	0.1752(5)	–0.1503(10)	0.2862(5)	0.017(4)	0.014(4)	0.010(4)	0.001(3)	0.002(3)	0.002(3)	0.0142(16)
	0.1955(4)	–0.1477(8)	0.2573(3)	0.027(3)	0.010(3)	0.015(3)	–0.002(2)	0.001(2)	–0.006(2)	0.0175(12)
	0.215(4)	–0.144(10)	0.301(5)							0.030(4)*
OH(1)	0.1882(5)	0.2010(12)	0.3662(5)	0.025(5)	0.025(5)	0.017(4)	–0.006(4)	0.010(4)	0.000(4)	0.0217(19)
	0.2113(4)	0.2034(9)	0.3345(3)	0.033(3)	0.018(3)	0.012(3)	–0.003(3)	–0.001(2)	–0.000(3)	0.0215(13)
	0.220(4)	0.218(10)	0.372(5)							0.030(4)*
OH(2)	0.3216(5)	0.0291(12)	0.3645(5)	0.022(5)	0.026(5)	0.016(4)	–0.003(4)	0.005(3)	0.000(4)	0.0217(19)
	0.3608(4)	0.0276(9)	0.3080(4)	0.020(3)	0.032(4)	0.021(3)	0.003(3)	–0.007(2)	0.001(3)	0.0254(14)
	0.381(4)	0.020(10)	0.387(5)							0.030(4)*
OH(3)	0.7614(5)	0.0620(11)	0.2932(5)	0.014(4)	0.015(4)	0.016(4)	0.002(3)	0.007(3)	–0.003(3)	0.0144(16)
	0.7301(4)	0.0641(8)	0.3332(3)	0.016(3)	0.022(3)	0.016(3)	0.004(3)	–0.001(2)	–0.004(2)	0.0185(13)
	0.709(4)	0.079(10)	0.278(5)							0.030(4)*
OW(1)	0.3467(5)	0.0898(13)	0.5341(5)	0.027(5)	0.036(5)	0.016(4)	–0.000(4)	0.012(4)	–0.006(4)	0.025(2)
	0.3937(4)	0.1019(10)	0.4741(4)	0.028(3)	0.044(5)	0.020(3)	0.003(3)	0.009(3)	–0.009(3)	0.0300(16)
	0.418(4)	0.139(10)	0.565(5)							0.030(4)*
OW(2)	0.3683(5)	0.1915(11)	0.7035(5)	0.017(4)	0.013(4)	0.020(4)	–0.003(3)	0.000(3)	0.001(3)	0.0180(18)
	0.4074(4)	0.2091(9)	0.6386(4)	0.035(3)	0.010(3)	0.035(4)	0.001(3)	–0.016(3)	–0.003(3)	0.0291(15)
	–	–	–							–
OW(3)	0.7410(6)	0.1067(14)	0.0868(6)	0.039(6)	0.038(6)	0.040(6)	–0.023(5)	0.017(5)	–0.003(5)	0.038(3)
	0.6958(6)	0.1002(13)	0.1364(5)	0.055(5)	0.063(6)	0.056(5)	–0.031(5)	0.011(4)	–0.016(4)	0.058(2)
	0.664(5)	0.127(13)	0.072(6)							0.06(2)
OW(4)	0.4657(6)	0.1670(14)	0.0681(6)	0.036(6)	0.042(6)	0.029(5)	–0.005(4)	0.013(4)	0.011(5)	0.035(2)
	–	–	–	–	–	–	–	–	–	–
	–	–	–							–
OW(5)	0.5819(7)	0.1861(16)	–0.0150(7)	0.046(7)	0.047(7)	0.040(6)	0.004(5)	0.021(5)	–0.004(5)	0.043(3)
	–	–	–	–	–	–	–	–	–	–
	–	–	–							–

* Constrained to be equal during refinement.

Downloaded from https://pubs.geoscienceworld.org/canmin/article-pdf/57/5/605/4851376/i1499-1276-57-5-605.pdf
by University of Arizona user

TABLE 5. SELECTED INTERATOMIC DISTANCES (Å) IN TAMBOITE (T), METATAMBOITE (MT), AND LOWER HYDRATE (LH)

	(T)	(MT)	(LH)		(T)	(MT)	(LH)
Te(1)–O(5)	1.864(7)	1.865(5)	1.79(7)	*Te*(2)–O(8)	1.866(8)	1.869(5)	1.85(7)
Te(1)–O(6)	1.874(8)	1.873(5)	1.84(6)	*Te*(2)–O(9)	1.880(7)	1.879(6)	1.89(6)
Te(1)–O(7)	1.933(7)	1.938(5)	1.89(7)	*Te*(2)–O(10)	1.959(7)	1.936(5)	1.99(7)
Te(1)–O(6)	2.862(8)	2.869(5)	2.85(6)	*Te*(2)–O(3)	2.961(8)	2.818(6)	2.89(7)
Te(1)–O(8)	3.690(9)	3.638(6)	3.72(8)	*Te*(2)–O(4)	3.691(8)	3.813(6)	3.59(7)
Te(1)–O(9)	2.539(8)	2.568(6)	2.42(7)	*Te*(2)–O(5)	3.047(8)	3.059(6)	3.15(7)
Te(1)–O(13)	3.276(8)	3.247(5)	3.24(7)	*Te*(2)–O(6)	3.843(7)	3.815(6)	3.77(7)
Te(1)–OH(1)	3.223(8)	3.140(6)	3.20(6)	*Te*(2)–O(7)	3.003(7)	2.989(6)	3.16(6)
Te(1)–OH(3)	3.631(8)	3.638(5)	3.70(7)	*Te*(2)–O(7)	3.759(8)	3.771(5)	3.75(5)
				Te(2)–OH(3)	3.727(8)	3.714(6)	3.65(7)
Te(3)–O(11)	1.872(7)	1.852(5)	1.85(7)	*Te*(2)–OW(3)	2.594(10)	2.716(8)	2.83(7)
Te(3)–O(12)	1.906(7)	1.891(5)	1.87(7)				
Te(3)–O(13)	1.915(7)	1.913(5)	2.00(7)	*Te*(4)–O(14)	1.864(8)	1.843(6)	1.87(7)
Te(3)–O(6)	2.855(8)	2.804(5)	2.84(6)	*Te*(4)–OH(1)	1.913(8)	1.916(6)	1.94(6)
Te(3)–O(8)	2.955(8)	2.897(6)	2.98(7)	*Te*(4)–OH(2)	1.921(8)	1.918(5)	1.93(7)
Te(3)–O(11)	3.246(7)	3.247(6)	3.32(7)	*Te*(4)–O(2)	3.737(9)	3.771(7)	3.42(6)
Te(3)–O(12)	2.826(8)	2.821(5)	2.82(7)	*Te*(4)–O(3)	2.852(9)	2.907(7)	2.86(6)
Te(3)–O(13)	3.209(8)	3.187(6)	3.24(7)	*Te*(4)–O(5)	3.601(8)	3.573(5)	3.59(7)
Te(3)–O(14)	2.978(8)	2.937(6)	3.06(5)	*Te*(4)–O(10)	3.112(7)	3.052(5)	3.18(7)
Te(3)–OH(1)	3.547(9)	3.538(6)	3.47(7)	*Te*(4)–O(11)	3.602(8)	3.586(6)	3.59(7)
				Te(4)–O(12)	2.646(8)	2.619(5)	2.68(6)
Fe(1)–O(7)	2.050(7)	2.026(5)	2.05(7)	*Te*(4)–OH(3)	3.760(8)	3.762(6)	3.84(7)
Fe(1)–O(7)	2.058(7)	2.052(5)	2.16(7)	*Te*(4)–OW(2)	3.588(8)	3.447(7)	–
Fe(1)–O(8)	1.951(8)	1.946(6)	1.95(6)				
Fe(1)–O(10)	2.052(7)	2.061(5)	2.08(6)	*Fe*(2)–O(6)	2.046(8)	2.050(6)	2.13(8)
Fe(1)–O(12)	1.988(7)	1.975(5)	2.03(7)	*Fe*(2)–O(10)	2.003(8)	2.015(5)	2.04(7)
Fe(1)–O(13)	2.068(8)	2.048(5)	1.95(7)	*Fe*(2)–O(11)	1.962(7)	1.963(6)	1.94(7)
<*Fe*(1)–O>	2.028	2.018	2.04	*Fe*(2)–O(13)	2.178(8)	2.169(5)	2.22(6)
				Fe(2)–O(14)	2.058(8)	2.033(6)	2.09(8)
Fe(3)–O(4)	2.021(8)	2.003(6)	2.11(7)	*Fe*(2)–OH(3)	1.960(8)	1.951(5)	1.98(6)
Fe(3)–O(5)	1.960(8)	1.950(6)	1.92(7)	<*Fe*(2)–φ>	2.035	2.030	2.07
Fe(3)–O(9)	1.986(8)	1.979(5)	1.96(7)				
Fe(3)–OH(3)	1.996(8)	1.984(5)	2.00(6)	*S*–O(1) / OH(4)	1.453(10)	1.422(8)	1.64(7)
Fe(3)–OW(1)	2.045(8)	2.068(6)	2.01(6)	*S*–O(2)	1.484(9)	1.474(7)	1.41(7)
Fe(3)–OW(2)	2.044(8)	2.033(6)	–	*S*–O(3)	1.487(9)	1.478(7)	1.49(6)
Fe(3)–O(2)	–	–	2.08(7)	*S*–O(4)	1.503(8)	1.482(7)	1.47(8)
<*Fe*(3)–φ>	2.009	2.003	2.01	<*S*–φ>	1.482	1.464	1.50

[OH(1), OH(2)] form single strong bonds to Te(4), and OH(3) is shared by Fe(2) and Fe(3).

In tamboite, there are five OW sites that the valence-sum rule indicates are each occupied by H_2O. The OW(1) and OW(2) groups are each bonded to one Fe^{3+} and the OW(3) group is weakly bonded to Te^{4+} (Table 6). The OW(4) and OW(5) groups are not bonded to any cation (except H^+) and are held in the structure solely by hydrogen bonds.

In metatamboite (Table 7), there are three OW sites that the valence-sum rule indicates are each occupied by (H_2O): OW(1), OW(2), and OW(3), which have the same bonding environments to the non-H cations as the corresponding (H_2O) groups in tamboite. Interstitial {H_2O} groups are absent in metatamboite.

Bond Topology

The structures of tamboite and metatamboite are based on virtually identical ferric-sulfate-tellurite-hydrate slabs that are constructed from strands of ferric-sulfate-hydrate polyhedra linked by Te^{4+} cations. The strand from metatamboite is shown in Figure 7. Two adjacent Fe(1) octahedra share an edge with each other at the core, and the Fe(1) octahedron shares an edge with an adjacent Fe(2) octahedron. The Fe(2) octahedron shares a vertex [OH(3)] with an Fe(3)

Downloaded from https://pubs.geoscienceworld.org/canmin/article-pdf/57/5/605/4851376/i1499-1276-57-5-605.pdf
by University of Arizona user

TABLE 6. BOND-VALENCE (*vu*) VALUES FOR TAMBOITE

	Te(1)	*Te*(2)	*Te*(3)	*Te*(4)	*Fe*(1)	*Fe*(2)	*Fe*(3)	*S*	Σ	H(1)	H(2)	H(3)	H(4)	H(5)	H(6)	H(7)	H(8)	H(9)	H(10)	H(11)	H(12)	H(13)	Σ
O(1)								1.57	1.57						**0.2**						**0.1**		1.87
O(2)				0.01				1.46	1.47		0.2	0.05							**0.2**				1.92
O(3)		0.08		0.10				1.45	1.63			0.05				0.2							1.88
O(4)		0.01					0.49	1.39	1.89														1.89
O(5)	1.28	0.06		0.01			0.58		1.93														1.93
O(6)	1.25	0.01	0.10			0.46			1.92														1.92
	0.10																						
O(7)	1.07	0.07			0.45				2.04														2.04
		0.01			0.44																		
O(8)	0.01	1.27	0.08		0.60				1.96														1.96
O(9)	0.23	1.20					0.54		1.97														1.97
O(10)		1.00		0.05	0.45	0.52			2.02														2.02
O(11)			1.25	0.01		0.58			1.88	0.05													1.93
			0.04																				
O(12)			1.15	0.17	0.54				1.97														1.97
			0.11																				
O(13)	0.03		1.12		0.43	0.32			1.94														1.94
			0.04																				
O(14)			0.07	1.28		0.44			1.79									0.15					1.94
OH(1)	0.04		0.02	1.13					1.19	0.9													2.09
OH(2)				1.11					1.11		0.8			0.2									2.11
OH(3)	0.01	0.01		0.01		0.58	0.53		1.14			0.9											2.04
OW(1)							0.46		0.46				0.8	0.8									2.06
OW(2)				0.02			0.46		0.48						0.8	0.8							2.08
OW(3)		0.20							0.20	0.05							0.8	0.85					1.90
OW(4)									0				**0.2**						0.8	0.85		0.2	2.05
OW(5)									0								**0.2**			0.15	0.9	0.8	2.05
Σ	4.02	3.92	3.98	3.90	3.01	2.90	3.06	5.87		1.0	1.0	1.0	1.0	1.0	1.0	1.0	1.0	1.0	1.0	1.0	1.0	1.0	

Inter-slab hydrogen bonds are bolded.

Downloaded from https://pubs.geoscienceworld.org/canmin/article-pdf/57/5/605/4851376/i1499-1276-57-5-605.pdf
by University of Arizona user

TABLE 7. BOND-VALENCE (*vu*) VALUES FOR METATAMBOITE

	Te(1)	*Te*(2)	*Te*(3)	*Te*(4)	*Fe*(1)	*Fe*(2)	*Fe*(3)	*S*	Σ	H(1)	H(2)	H(3)	H(4)	H(5)	H(6)	H(7)	H(8)	H(9)	Σ
O(1)								1.70	1.70								**0.2**		1.90
O(2)				0.01				1.49	1.50		0.2	0.05			**0.2**				1.95
O(3)		0.11		0.09				1.48	1.68			0.05				0.2			1.93
O(4)		0.01					0.52	1.46	1.99				**0.1**						2.09
O(5)	1.28	0.06		0.02			0.60		1.96										1.96
O(6)	1.25	0.01	0.11			0.45			1.92										1.92
	0.10																		
O(7)	1.06	0.07			0.49				2.08										2.08
		0.01			0.45														
O(8)	0.01	1.26	0.09		0.61				1.97										1.97
O(9)	0.21	1.23					0.55		1.99										1.99
O(10)		1.06		0.06	0.44	0.50			2.06										2.06
O(11)			1.32	0.02		0.58			1.96										1.96
			0.04																
O(12)			1.19	0.18	0.56				2.04										2.04
			0.11																
O(13)	0.04		1.13		0.46	0.33			2.00										2.00
			0.08																
O(14)			0.02	1.35		0.48			1.91									0.05	1.96
OH(1)	0.05			1.12					1.19	0.9				0.1					2.19
OH(2)				1.11					1.11		0.8							0.05	1.96
OH(3)	0.01	0.01		0.01		0.60	0.55		1.18			0.9							2.08
OW(1)							0.43		0.43				0.9	0.9					2.23
OW(2)				0.02			0.48		0.50						0.8	0.8			2.10
OW(3)		0.14							0.14	0.1							0.8	0.9	1.94
Σ	4.01	3.97	4.13	3.99	3.01	2.94	3.13	6.13		1.0	1.0	1.0	1.0	1.0	1.0	1.0	1.0	1.0	

Inter-slab hydrogen bonds are bolded.

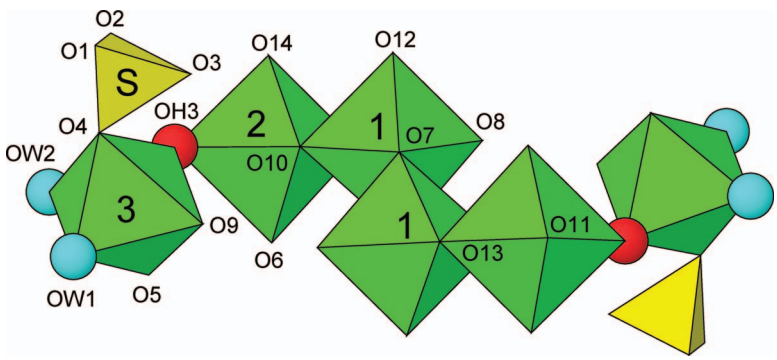

FIG. 7. The $[Fe^{3+}{}_3(SO_4)O_{10}(OH)(H_2O)_2]_2$ ferric-sulfate-hydrate strand in metatamboite. Green polyhedra: $Fe^{3+}\Phi_6$ octahedra; yellow polyhedra: $S^{6+}O_4$ tetrahedra; red circle: (OH) group; blue circle: (H_2O) group.

octahedron, and the Fe(3) octahedron links to the (SO_4) group *via* the O(4) anion. Two (H_2O) groups [OW(1), OW(2)] are attached to the Fe(3) atom at the outer margin of the strand. The result is a convoluted fragment of a chain of composition $[Fe^{3+}{}_3(SO_4)O_{10}(OH)(H_2O)_2]^{14-}{}_2$ (Fig. 7).

The strands of ferric-sulfate-hydrate polyhedra are decorated by $Te\Phi_3$ pyramids that bind neighboring strands to form a complicated (100) slab of composition $Fe^{3+}{}_3(SO_4)(Te^{4+}O_3)_3(Te^{4+}O(OH)_2)(OH)(H_2O)_3$ (Fig. 8); note that the 10 simple O^{2-} anions (that bond to Fe^{3+} and not S^{6+}) within the strand described above also link to Te^{4+} ions *via* strong bonds and are now

Downloaded from https://pubs.geoscienceworld.org/canmin/article-pdf/57/5/605/4851376/i1499-1276-57-5-605.pdf
by University of Arizona user

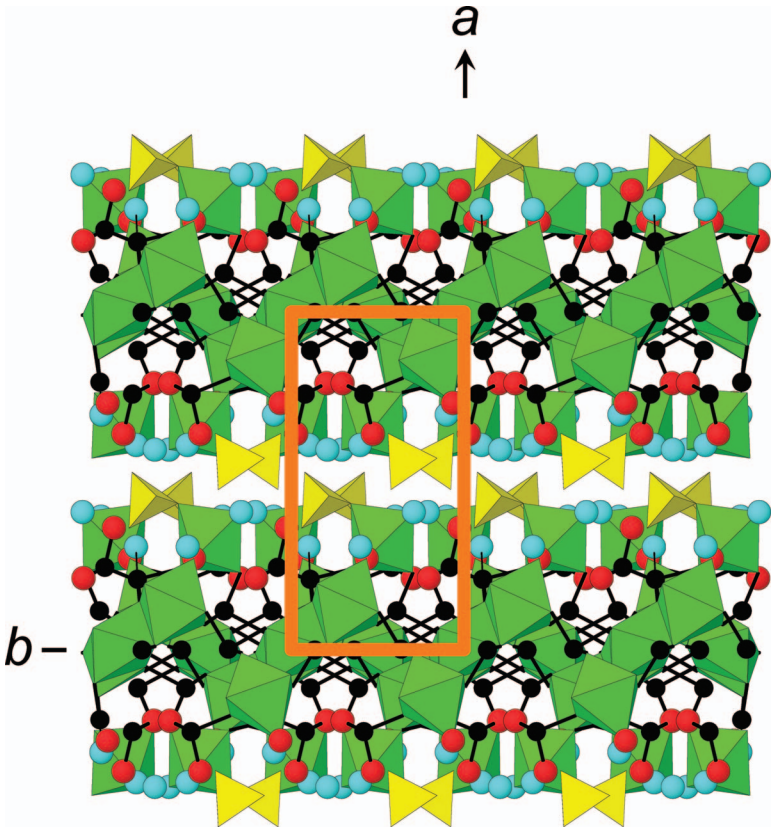

FIG. 8. Adjacent structural (100) slabs in metatamboite projected down [001]. Legend as in Figure 7; black circles: Te atoms; thick black lines: strong Te–Φ bonds; thin black lines: weaker Te(2)–OW(3) bonds; orange rectangle: unit-cell outline.

grouped as such. In addition to the H-bearing anion groups belonging to the strand, the slab also contains: (1) two additional (OH) groups attached to the Te(4) cation [OH(1), OH(2)] and (2) an additional (H_2O) group [OW(3)] weakly bonded to Te(2) (Table 5). The chemical formula of the slab is the complete formula-unit for metatamboite, and the formula unit for tamboite differs only in terms of two additional interstitial {H_2O} groups [OW(4), OW(5)] within the interstitial gap between slabs. Viewed down the **b** axis, the slab is formed of columns of strands of ferric-sulfate-hydrate (seen end-on in Fig. 9) decorated by $Te\Phi_3$ pyramids (weaker Te–Φ bonds are not shown in order to highlight individual strands). A single [010] column [seen in profile projected onto $(10\bar{2})$] shows the inclination of the strands relative to [010] (Fig. 10). Note that adjacent columns within a given slab are inclined to each other (Fig. 9) in relation to the 2_1-screw symmetry operator (along [010] midway between the columns), imparting a zig-zag appearance to the strands when viewed down [001] (Fig. 8).

The intra-slab character is similar in metatamboite and tamboite, although the relative position of adjacent slabs viewed down [010] differs markedly in the two minerals (Fig. 9). In metatamboite, the serrated bounding surfaces of adjacent (100) slabs fit tightly together with only hydrogen bonds (not shown) bridging the narrow interstitial gap (Fig. 9a). In tamboite, adjacent slabs are further apart with the resulting inter-slab opening filled by two interstitial {H_2O} groups *pfu* (Fig. 9b). The expansion of the space between slabs in tamboite is perpendicular to the central axis of the strand in the $(10\bar{2})$ plane, and ~3.6 Å of sinistral displacement results in a ~2.6 Å increase in the *a* cell parameter and a ~10° increase in the β angle for tamboite (Table 3). The volume of a single H_2O group is ~30 $Å^3$, calculated from the density of water at room temperature. Tamboite contains two interstitial {H_2O} groups *pfu* that are not present in metatamboite, and tamboite has a unit-cell volume that is greater by 255 $Å^3$ (Table 3). The interstitial {H_2O} groups in tamboite are well ordered and refine to full

Downloaded from https://pubs.geoscienceworld.org/canmin/article-pdf/57/5/605/4851376/i1499-1276-57-5-605.pdf
by University of Arizona user

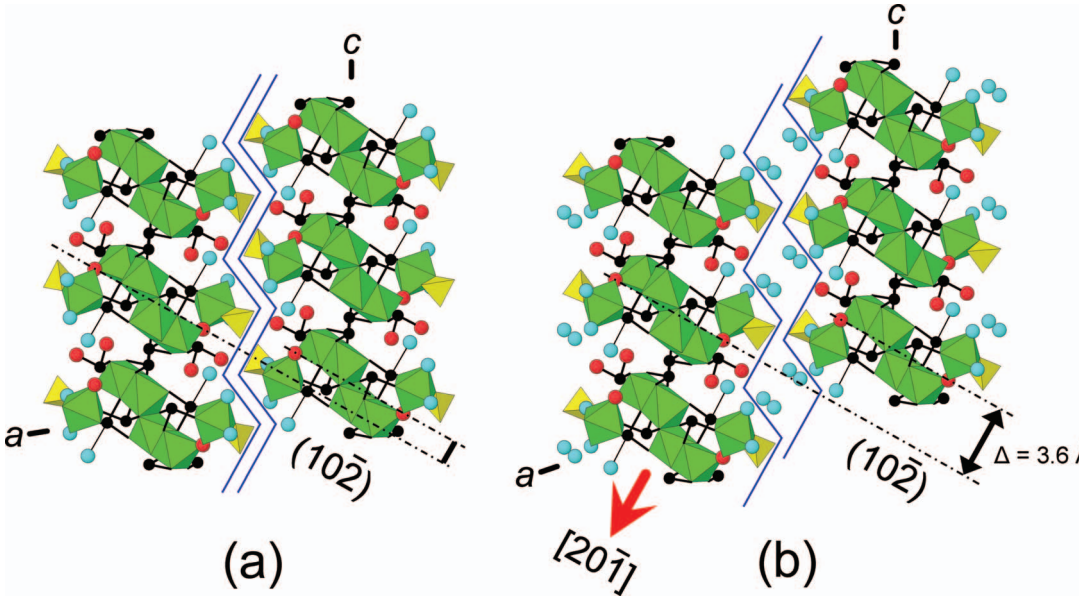

FIG. 9. Adjacent structural (100) slabs viewed down [010], comprised of vertical columns (along [010]) of strands in: (a) metatamboite, (b) tamboite. Legend as in Figures 7 and 8; staircased purple lines mark (100) slab boundaries; black dashed lines: construction lines passing through central axes of columns; red arrow: slab-displacement direction.

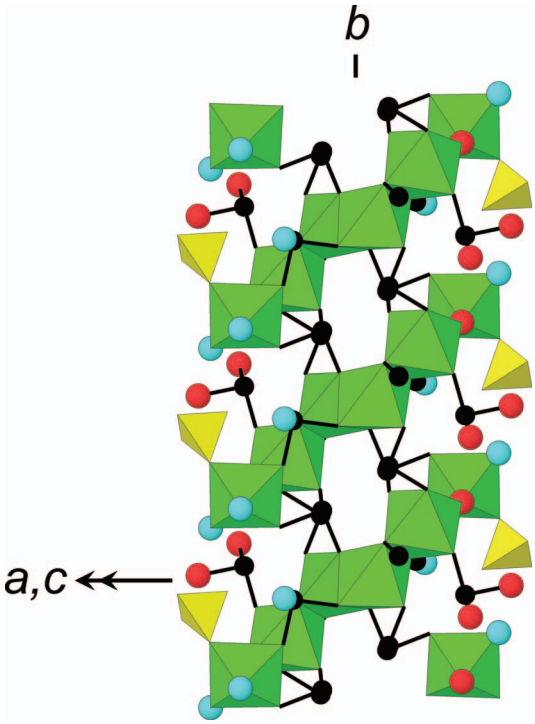

FIG. 10. An isolated column of strands in metatamboite projected onto (10$\bar{2}$).

site-occupancy. The larger observed unit-cell volume for tamboite corresponds to a 31.9 Å^3 volume increase per interstitial {H_2O} group, which is in good agreement with the above-estimated ~30 Å^3 volume of an individual H_2O group. For both structures, the Te(4)Φ_3 pyramid containing the two terminal (OH) groups and the (H_2O) group [OW(3)] that is weakly bonded to Te(2) are located near the periphery of the slab (Fig. 9) and are involved in a combination of intra- and inter-slab hydrogen-bonding.

HYDROGEN BONDING

The H atoms in tamboite and metatamboite could not be reliably located in the difference-Fourier maps during structure refinement. However, a reasonably unambiguous hydrogen-bonding scheme was determined for both structures from consideration of the relative anion (O_D, O_A) positions and bond-valence deficiencies (Tables 6 and 7). We used the latest bond-valence equations for Te^{4+}–O, Fe^{3+}–O, and S^{6+}–O bonds in order to achieve the most reliable bond-valence summations at the anions (Gagné & Hawthorne 2015); this was particularly important for anions coordinating Te^{4+} over distances from 1.843 to 3.843 Å. We elected to include all contacts between Te^{4+} and O that are <3.9 Å; these 82 individual Te^{4+}–O distances in tamboite and metatamboite are plotted against their calculated bond-valences (Fig. 11). There

Downloaded from https://pubs.geoscienceworld.org/canmin/article-pdf/57/5/605/4851376/i1499-1276-57-5-605.pdf
by University of Arizona user

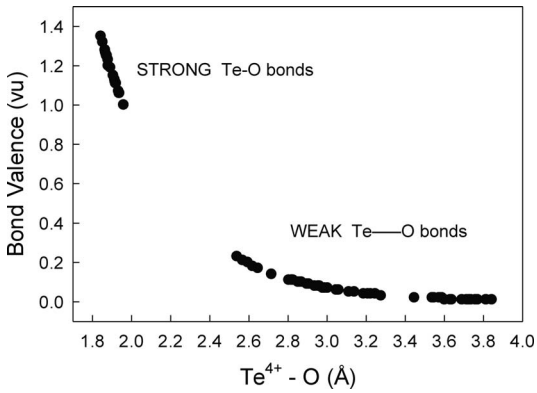

FIG. 11. The 82 (Te^{4+}–O < 3.9 Å) bonds in tamboite and metatamboite plotted against the calculated bond-valence (Gagné & Hawthorne 2015).

are two distinct bond-length populations: short (1.84–1.96 Å) strong (1.36–1.00 *vu*) bonds and long (2.54–3.84 Å) weak (0.23–0.01 *vu*) bonds. In producing a revised set of bond-valence parameters for Te^{4+}–O, Mills & Christy (2013) considered Te^{4+}–O bonds to a cutoff of 3.5 Å that included Te^{4+} coordination numbers from [3] to [12]. The Te^{4+} coordinations in tamboite and metatamboite (for Te^{4+}–O < 3.9 Å) range from [9] to [11] (Table 5). Following the arguments of Gagné & Hawthorne (2015), we have elected to include Te^{4+}–O bonds to <3.9 Å (Tables 5, 6, and 7). We note that the Te^{4+}–O bonds in the range 3.5–3.9 Å individually contribute ≤0.02 *vu* to a particular anion. The inclusion of all Te^{4+}–O bonds <3.9 Å in tamboite and metatamboite results in bond valence sums of 3.90–4.13 *vu* at the *Te* sites (Tables 6 and 7). The bond-valence sums for the three *Fe* sites in tamboite and metatamboite span 2.90–3.06 *vu* and 2.94–3.13 *vu*, and the incident bond-valences at the *S* sites are 5.87 and 6.13 *vu*, respectively. All bond-valence sums around the *Te*, *Fe*, and *S* sites are near their ideal values of 4, 3, and 6, respectively. We therefore regard the bond-valence sums at the coordinating oxygen atoms (excluding any contribution from H atoms) to reliably indicate reasonable accord with the valence-sum rule (*i.e.*, ~2 *vu*) for some anions, and a significant incident bond-valence deficiency (*i.e.*, especially < ~1.8 *vu*) for other anions; the latter group are thereby classed as probable hydrogen-bond acceptors (O_A). The environment surrounding each hydrogen-bond donor anion (O_D) was carefully inspected for geometrically favorable hydrogen-bond arrangements using the following criteria: (1) $O_D \cdots O_A$ distances extend to a maximum of 3.4 Å, and (2) O_A–O_D–O_A angles lie within 80–140° for H_2O groups. Additionally, hydrogen-bonding arrangements involving O_D and O_A anions along a polyhedron edge were generally avoided; however, in the case of Te^{4+}, some very long Te^{4+}–O contacts were considered as possible O_D or O_A anions (*i.e.*, for possible $O_D \cdots O_A$ anions, the anion furthest from a given Te atom is at least 3.44 Å from that Te atom). In both the tamboite and metatamboite structures, the O^{2-} ions with the lowest incident bond-valence sums are O(1), O(2), and O(3) belonging to the (SO_4) group, with sums ranging from 1.47 to 1.70 *vu* (Tables 6 and 7). Assignment of hydrogen bonds began with the identification of potential O_D anions for these O_A anions. This analysis provided several unambiguous hydrogen bonds that were used as a starting basis. Subsequent recognition of hydrogen bonds was complicated by the number of geometrically possible O_A anions. The remaining O^{2-} ions [*i.e.*, O(4) to O(14)] have incident bond-valence sums from 1.79 to 2.08 *vu* for both tamboite and metatamboite, and all were initially considered as possible acceptors of weak hydrogen bonds. For both tamboite and metatamboite, the complex ligands (*i.e.*, OH and H_2O groups) that are bonded to cations are similarly coordinated in the two structures: (1) the OH(1) and OH(2) anions each form a single strong bond (~1.1 *vu*) with *Te*(4), whereas the OH(3) anion receives a comparable total bond-valence from two neighboring Fe^{3+} ions; (2) the OW(1) and OW(2) anions each form a moderately strong bond (~0.46 *vu*) with Fe(3), whereas the OW(3) anion forms a relatively weak bond (~0.17 *vu*) with Te(2). These stereochemical differences between the (OH) and (H_2O) groups suggest the OH(1), OH(2), and OW(3) groups as more likely candidates to receive a weak hydrogen bond. Among the (OH) groups, the OH(3) anion is [3]-coordinated [*i.e.*, bonded to Fe(2) and Fe(3), and H^+], whereas the OH(1) and OH(2) anions are only [2]-coordinated [*i.e.*, bonded strongly to Te(4) and H^+], making OH(3) a less likely candidate for a hydrogen-bond acceptor anion. The higher incident bond-valence at the OW(1) and OW(2) anions (~0.46 *vu*) significantly reduces the likelihood of additional incident hydrogen bonds. However, the relatively weak incident bond-valence at the OW(3) anion (~0.17 *vu*) allows another possible weak hydrogen bond. The tamboite structure (but not the metatamboite structure) contains two interstitial {H_2O} groups, OW(4) and OW(5), that each donate two hydrogen bonds and also likely accept two hydrogen bonds in an approximate tetrahedral geometry. Thus the list of potential hydrogen-bond acceptor anions for both structures is as follows: O(1)–O(3) {probable}, O(4)–O(14) {possible, especially O(14) in tamboite with a lower bond-valence sum of 1.79 *vu*}, OH(1) and OH(2) {possible}, OW(3) {possible}, and OW(4)–OW(5) {probable; tamboite only}. The num-

Downloaded from https://pubs.geoscienceworld.org/canmin/article-pdf/57/5/605/4851376/i1499-1276-57-5-605.pdf
by University of Arizona user

TABLE 8. PROPOSED HYDROGEN BONDING* FOR TAMBOITE AND METATAMBOITE

Tamboite		Metatamboite	
OH(1)···OW(3)	3.201(14)	OH(1)···OW(3)	3.194(11)
OH(1)···O(11)	2.847(11)		
OH(2)···O(2)	2.732(12)	OH(2)···O(2)	2.684(10)
OH(3)···O(2)	2.923(12)	OH(3)···O(2)	3.146(11)
OH(3)···O(3)	3.274(12)	OH(3)···O(3)	3.159(9)
OW(1)···OW(4)	**2.612(13)**	**OW(1)···O(4)**	**2.932(8)**
OW(1)···OH(2)	2.756(11)	OW(1)···OH(1)	3.291(9)
OW(4)–OW(1)–OH(2)	100.6(4)	O(4)–OW(1)–OH(1)	109.5(2)
OW(2)···O(1)	**2.708(12)**	**OW(2)···O(2)**	**2.676(9)**
OW(2)···O(3)	2.689(12)	OW(2)···O(3)	2.654(9)
O(1)–OW(2)–O(3)	122.3(4)	O(2)–OW(2)–O(3)	101.6(3)
OW(3)···OW(5)	**2.748(15)**	**OW(3)···O(1)**	**2.745(11)**
OW(3)···O(14)	2.778(12)	OW(3)···OH(2)	3.384(11)
OW(5)–OW(3)–O(14)	119.7(5)	OW(3)···O(14)	2.834(10)
		O(1)–OW(3)–OH(2)	101.9(3)
OW(4)···O(2)	**2.751(13)**	O(1)–OW(3)–O(14)	139.1(4)
OW(4)···OW(5)	**2.762(16)**		
O(2)–OW(4)–OW(5)	123.8(5)		
OW(5)···O(1)	**3.381(14)**		
OW(5)···OW(4)	**2.757(14)**		
O(1)–OW(5)–OW(4)	120.7(4)		

* Distances (Å), angles (°); inter-slab hydrogen bonds are bolded.

ber of possible acceptor anions is large and no reliable H positions could be extracted from residual peaks in difference-Fourier maps. However, applying the geometric criteria given above, we were able to develop a reasonably unambiguous assignment of hydrogen bonds for both structures.

Assignment of hydrogen bonds in metatamboite

Of the four anions belonging to the (SO_4) group, the O(2) anion is the most bond-valence deficient (1.50 *vu*) and is expected to receive two strong hydrogen bonds (Table 7). There are only two available O_D anions that can donate strong hydrogen bonds to the O(2) anion: OW(2) and OH(2), both 2.68 Å from O(2). Thus we assign a hydrogen bond from OH(2) to O(2) (Table 8). The O(3) anion of the (SO_4) group has an incident-bond-valence sum of 1.68 *vu* and is expected to accept a strong hydrogen bond; the only available donor is the (H_2O) group at OW(2), 2.65 Å from O(3). Therefore the O(2) and O(3) anions [associated with spatially different (SO_4) groups] receive strong hydrogen bonds from a neighboring (H_2O) group at OW(2), and the favorable O(2)–OW(2)–O(3) angle of 101.6° supports this assignment. The O(1) anion of the (SO_4) group has an incident bond-valence sum of 1.70 *vu* and is expected to accept a strong hydrogen bond. The neighboring (H_2O) group at OW(3) is 2.74 Å away and is the only O_D available to form a strong hydrogen bond with O(1). Identification of more O_A anions in the structure from inspection of incident bond-valence alone is inconclusive: current adjusted incident bond-valences at O(1)–O(14) now span the range 1.88–2.08 *vu*, incident bond-valences at OH(1) and OH(2) (without contributions from H^+) are 1.19 and 1.11 *vu*, respectively, and the incident bond-valence at OW(3) (without contributions from H^+) is 0.14 *vu* from Te(2). Various combinations of possible hydrogen-bond arrangements indicate that the OH(1) and/or OH(2) anion must act as an O_A anion. Comparison of the OH(1) and OH(2) environments shows that the OH(2) anion has a lower overall coordination and slightly lower incident bond-valence and seems the more likely anion to accept a weak hydrogen bond. We therefore designate the OH(2) anion as an O_A and identify OW(1) or OW(3) as possible donor species. However, only the arrangement OH(2)–OW(3)–O(1) has a favorable O_A–O_D–O_A angle (*i.e.*, 101.9°), and hence we assign a weak hydrogen-bond from the (H_2O) group at OW(3) to the anion at OH(2). Note that the assigned hydrogen bond from OW(3) to OH(2) is a bifurcated hydrogen bond

Downloaded from https://pubs.geoscienceworld.org/canmin/article-pdf/57/5/605/4851376/i1499-1276-57-5-605.pdf
by University of Arizona user

that also involves the O(14) anion as the other O_A anion (this decision is based on a combination of geometry, incident bond-valence at O_A, and analogy with the similar environment in tamboite). An unambiguous assignment of hydrogen bonding with the (H_2O) group at OW(1) as the donor species is now possible, as the OH(2) anion is now excluded as a possible O_A [*i.e.*, OH(2) was previously assigned a hydrogen bond from OW(3)]. Of the three remaining possible O_A anions to accept hydrogen bonds from OW(1) [*i.e.*, O(1), O(4), OH(1)], only the arrangement O(4)–OW(1)–OH(1) has a favorable O_A–O_D–O_A angle: 109.5°. Hence, we assign weak hydrogen-bonds from the (H_2O) group at OW(1) to O(4) and OH(1). The remaining unassigned hydrogen bonds are those emanating from the (OH) groups at OH(1) and OH(3). The plausible O_A anions are: O(11), O(13), OW(3) and O(2), O(3), OW(3), respectively. We earlier identified OW(3) as a probable O_A for a single hydrogen bond [which would complete tetrahedral coordination about the OW(3) anion]. OH(1) and OH(3) are 3.19 and 3.20 Å from OW(3), and therefore initially seem equally likely candidates to donate this hydrogen bond to OW(3). However, when we compare the current incident-bond-valence sums of the other prospective O_A ions [*i.e.*, O(2) 1.90 *vu*, O(3) 1.88 *vu*, O(11) 1.96 *vu*, O(13) 2.00 *vu*], we see that application of the valence-sum rule favors the assignment of a weak hydrogen bond from OH(1) to OW(3) [*i.e.*, the incident-bond-valence at O(11) and O(13) are relatively concordant with the valence-sum rule] and a weak bifurcated hydrogen bond from OH(3) to O(2) and O(3) [*i.e.*, O(2) and O(3) then become more concordant with the valence-sum rule]. A hydrogen bond from OH(1) and OH(3) has been assigned accordingly (Table 8).

Assignment of hydrogen bonds in tamboite

The O(1), O(2), and O(3) anions of the (SO_4) group in tamboite have low incident bond-valence sums (*i.e.*, 1.47–1.63 *vu*) and are expected to receive several hydrogen bonds. From the available O_D possibilities, the O(1) and O(3) anions can receive only strong hydrogen bonds from the (H_2O) group at OW(2). The O(1)–OW(2)–O(3) angle is 122.3° and is the only arrangement with a favorable geometry, and we have assigned strong hydrogen bonds from OW(2) to O(1) and O(3) (Table 8). As in metatamboite, the O(2) anion of the (SO_4) group in tamboite has the lowest incident bond-valence sum of the sulfate ligands and is expected to accept two strong hydrogen bonds. The OH(2) and OW(4) anion groups are the only available O_D anions, and we assign strong hydrogen bonds from the (OH) group at OH(2) and the {H_2O} group at OW(4) to O(2). When considering possible hydrogen bonds from OW(4) to O(2) and another O_A, in conjunction with an approximate overall tetrahedral coordination about OW(4), only two O(2)–OW(4)–O_A arrangements are geometrically favorable: O(2)–OW(4)–OW(5) at 123.8° and O(2)–OW(4)–OW(1) at 115.9°. However, the latter involves the OW(1) anion receiving a hydrogen bond, which was earlier considered as unlikely for both structures because of the relatively strong Fe(3)–OW(1) bond. We therefore assign hydrogen bonds from the {H_2O} group at OW(4) to O(2) and OW(5). In turn, OW(1) and OW(5) are geometrically feasible O_D anions for the interstitial {H_2O} group at OW(4), providing an approximate tetrahedral coordination about OW(4). With one hydrogen bond from OW(5) to OW(4), there are two geometrically favorable OW(4)–OW(5)–O_A arrangements: (1) one involving O(1) with an O_A–O_D–O_A angle of 120.7°, and (2) the other involving OW(1) with an O_A–O_D–O_A angle of 116.5°. However, as stated above, the OW(1) anion is not expected to receive a hydrogen bond, and the currently bond-valence-deficient O(1) anion requires an additional hydrogen bond. We therefore assign hydrogen bonds from the interstitial {H_2O} group at OW(5) to OW(4) and O(1). To complete the tetrahedral coordination about the OW(5) anion, including the aforementioned hydrogen bond from a neighboring {H_2O} group at OW(4), the most plausible assignment is a hydrogen bond from a neighboring (H_2O) group at OW(3). We therefore assign a hydrogen bond from the (H_2O) group at OW(3) to OW(5).

Next, we examined the environment around OW(3) for a second O_A to receive the other hydrogen bond from the (H_2O) group at OW(3). There are three such anions [O(14), OH(1), OH(3)], all with acceptable OW(5)–OW(3)–O_A angles. The O(14) anion is notably bond-valence deficient (1.79 *vu*, Table 5) in tamboite, and the only feasible O_D is the (H_2O) group at OW(3); we therefore assign hydrogen bonds from the (H_2O) group at OW(3) to O(14) and OW(5), where the O(14)–OW(3)–OW(5) angle is 119.6°. The OW(3) anion forms a single weak bond to Te(2), and OW(3) is expected to accept a hydrogen bond. The (OH) group at OH(1) is the most geometrically favorable O_D to form a weak hydrogen bond to OW(3) and complete an approximate tetrahedral coordination about OW(3); a weak hydrogen bond was so assigned. The O(11) anion is also bond-valence deficient (1.88 *vu*, Table 5) and is in a geometrically favorable position to accept a hydrogen bond from OH(1); hence we assign a bifurcated hydrogen bond from OH(1) to OW(3) and O(11). We earlier assigned a hydrogen bond from the (H_2O) group at OW(1) to OW(4) but did not identify the other O_A anion for the (H_2O) group at OW(1). Both the OH(1) and OH(2) anions are in favorable positions;

Downloaded from https://pubs.geoscienceworld.org/canmin/article-pdf/57/5/605/4851376/i1499-1276-57-5-605.pdf
by University of Arizona user

however, the arrangement OW(1)–H···OH(2)–H···O(2) with an OW(1)–OH(2)–O(2) angle of 125.0° is preferred over the OW(1)–H···OH(1)–H···OW(3) arrangement with an OW(1)–OH(1)–OW(3) angle of 83.2°. We therefore assign hydrogen bonds from the (H_2O) group at OW(1) to OW(4) and OH(2). The only remaining unassigned hydrogen-bond is that involving OH(3). The O(2) and O(3) anions of a neighboring (SO_4) group are equally plausible hydrogen-bond acceptors, and we assign a bifurcated hydrogen bond from OH(3) to O(2) and O(3) (as was assigned in metatamboite).

Differences in hydrogen bonding in tamboite and metatamboite

It is necessary to identify the differences in hydrogen bonding between tamboite and metatamboite in order to understand the mechanism by which the reversible hydration-dehydration proceeds. The hydrogen bonds in these two minerals can be divided into two types: (1) intra-slab hydrogen bonds that provide additional linkage within the slab, and (2) inter-slab hydrogen bonds that bridge neighboring slabs. The intra-slab bonding is very similar in each structure, and we will focus upon the inter-slab hydrogen bonds that are involved in the insertion of two interstitial {H_2O} groups into the metatamboite structure to form the tamboite structure; the inter-slab hydrogen bonds are bolded in Tables 6 and 8.

Intra-slab hydrogen bonds from the (OH) groups

All three (OH) groups donate intra-slab hydrogen bonds at the margins of the slab in both structures (Figs. 8 and 9). The hydrogen bonds from the (OH) groups in tamboite (Fig. 12) differ only marginally from those in metatamboite: in metatamboite, the OH(1) group donates a single hydrogen bond to the OW(3) anion, whereas in tamboite it forms a bifurcated bond to OW(3) and O(11). In both structures, there is a bifurcated hydrogen bond from OH(3) to the acceptor anions O(2) and O(3).

Intra- and inter-slab hydrogen bonding involving bonded (H_2O) groups

The (H_2O) groups OW(1) and OW(2) are at the margins of the slab and are bonded to Fe(3) and Te(2), respectively. For each group, one hydrogen bond is directed back into the slab (Figs. 8 and 9) and the other hydrogen bond links to an adjacent slab (Fig. 13). In metatamboite, the OW(1) intra- and inter-slab O_A anions are OH(1) and O(4), respectively (Fig. 13a). In tamboite, the OW(1) intra- and inter-slab O_A anions are OH(2) and OW(4), respectively (Fig. 13b). In metatamboite, the OW(3) intra-slab O_A anions are O(14) and OH(2), and the OW(3) inter-slab O_A anion is O(1) (Fig. 13a). In tamboite, the OW(3) intra- and inter-slab O_A anions are O(14) and OW(5), respectively (Fig. 13b). These differences in hydrogen bonding are a result of the different relative positions of neighboring slabs in the two structures. Where the slabs are close together (metatamboite), the (H_2O) groups at OW(1) and OW(3) can bond directly to the nearby O(4) and O(1) anions of the (SO_4) group on the neighboring slab (Fig. 13a). Where the slabs are further apart (Fig. 9b), OW(1) and OW(3) can no longer link directly to the distant O(4) and O(1) anions of the neighboring slab and instead form hydrogen bonds with the interstitial {H_2O} groups at OW(4) and OW(5) (Fig. 13b). Coupled with the differences in O_A identities between the two minerals, there are also differences in intra-slab hydrogen bonding for the (H_2O) groups at OW(1) and OW(3). In both metatamboite and tamboite, the intra-slab hydrogen bond from OW(2) links to the O(3) anion of the nearby (SO_4) group on the same slab (Fig. 13a and 13b). The inter-slab hydrogen bond from OW(2) links to an anion of an (SO_4) group on an adjacent slab. However, the specific anion of the (SO_4) group is different in the two minerals: O_A in metatamboite is O(2) (Fig. 13a), whereas O_A in tamboite is O(1) (Fig. 13b).

Inter-slab hydrogen bonds from interstitial {H_2O} groups in tamboite

The interstitial {H_2O} groups occupying the inter-slab region in tamboite are OW(4) and OW(5) (Fig. 9b). These two {H_2O} groups refine to full occupancy and are positionally well-ordered, together constituting two {H_2O} groups *pfu* in tamboite. Both the OW(4) and OW(5) anions are tetrahedrally coordinated, each donating two hydrogen bonds and accepting two hydrogen bonds (Tables 6 and 8). The interstitial {H_2O} groups at OW(4) and OW(5) accept hydrogen bonds from (H_2O) groups at OW(1) and OW(3) (Fig. 13b) and also from other interstitial {H_2O} groups at OW(4) and OW(5) (Fig. 14).

Two OW(4) and two OW(5) {H_2O} groups collectively form an $\{H_2O\}_4$ cluster. In this cluster, each {H_2O} group at OW(4) accepts a hydrogen bond from a neighboring {H_2O} group at OW(5), and each {H_2O} group at OW(5) accepts a hydrogen bond from a neighboring {H_2O} group at OW(4). The role of this $\{H_2O\}_4$ cluster is to propagate hydrogen bonding across interstitial space to more distant anions (Hawthorne 1992) in an adjacent slab. In metatamboite, adjacent slabs link directly through hydrogen bonds from (H_2O) groups of one slab to the O(1) and O(2) anions of the (SO_4) group in an adjacent slab

Downloaded from https://pubs.geoscienceworld.org/canmin/article-pdf/57/5/605/4851376/i1499-1276-57-5-605.pdf
by University of Arizona user

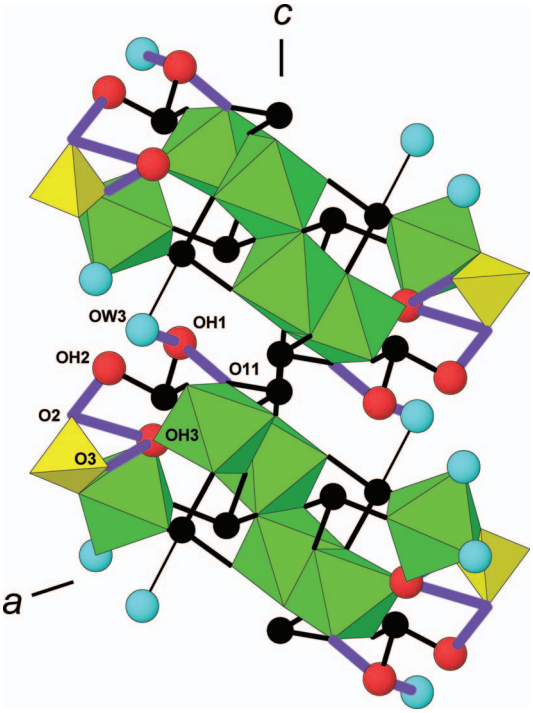

FIG. 12. The intra-slab hydrogen-bonds (thick purple lines) involving the (OH) groups in tamboite, structure projected down [010].

(Fig. 13a). In tamboite, linkage between adjacent slabs involves hydrogen-bond propagation *via* the $\{H_2O\}_4$ cluster (Fig. 14).

The $\{H_2O\}_4$ cluster

An isolated $\{H_2O\}_4$ cluster from tamboite is shown in Figure 15. The OW(4) and OW(5) anions form a square (2.76 Å on a side) with OW(4)–OW(5)–OW(4) and OW(5)–OW(4)–OW(5) angles of 86.1 and 93.9°, respectively. The plane is centered at coordinates (0.5,0.5,0.5) and the arrangement has $\bar{1}$ symmetry. The in-plane hydrogen bonding directionally propagates around the ring, and the out-of-plane hydrogen bonding is directed up or down relative to the plane of the ring in an uudd configuration (Hawthorne 2015) toward the O(1) and O(2) acceptor anions of the neighboring (SO_4) groups. Many experimental and theoretical studies have focused on understanding the structure of small water clusters, $(H_2O)_n$, with $n = 3$–5 (*e.g.*, Day *et al.* 2005, Dunn *et al.* 2004, Maheshwary *et al.* 2001, Shields *et al.* 2010, and references within). The $\{H_2O\}_4$ cluster in the crystal structure of tamboite is referred to as the C_i (or $\bar{1}$) cyclic tetramer $(H_2O)_{n=4}$. It has homodromic hydrogen bonding (*i.e.*, sequential donor–acceptor arrangements between water molecules around the ring), and the observed OW(4)–OW(5) distances in tamboite fall within the model distances for a cyclic tetramer reported in the literature (2.73–2.79 Å). There are two lowest-energy square-planar cyclic tetramers exhibiting homodromic hydrogen bonding: the S_4 ($\bar{4}$ symmetry) tetramer in which the out-of-plane H^+ ions are in the udud arrangement, and the C_i tetramer in which the out-of-plane H^+ ions are in the uudd arrangement. In isolated form, the S_4 tetramer has a slightly lower free-energy due to slightly lower H–H repulsion. However, both are common in the Earth's lower atmosphere under more humid conditions; on a humid day in the lower troposphere, the number of cyclic tetramers is estimated at 10^{11} clusters/cm^3). Thus, with the established abundance of cyclic-tetramer water clusters under humid conditions, we surmise that the dynamic metatamboite → tamboite conversion is ameliorated at higher relative humidity by both the increased availability of the $\{H_2O\}_4$ cluster at the crystal's surface and its suitability as a propagator of hydrogen bonds within the interstitial region of the structure. This absorption of $\{H_2O\}_4$ clusters is depicted in Figure 16, where atmospheric $\{H_2O\}_4$ clusters are shown entering and exiting the [010] channels between columns of SO_4 tetrahedra within the (100) plane (*cf.* Fig. 9). Within a given channel, the $\{H_2O\}_4$ clusters arrange themselves with their out-of-plane hydrogen bonds directed toward the O(1) and O(2) anions of the (SO_4) groups. The transient residency of these $\{H_2O\}_4$ clusters is apparently governed by the activity of $\{H_2O\}_4$ clusters surrounding the crystal. An SEM image of a tamboite/metatamboite crystal shows a uniform single flattened prism adjoining an assemblage of twisted fibers (Fig. 3). This transitional morphology can be rationalized by inhibited uptake of $\{H_2O\}_4$ clusters at greater distance along [010] from the crystal surface. In a sketch of an individual fiber tip (Fig. 17), atmospheric $\{H_2O\}_4$ clusters are shown entering the end of the prism along [010] with an accompanying left-lateral shear (along $[20\bar{1}]$) (*i.e.*, complete metatamboite → tamboite transition at higher humidity within the crystal tip) (*cf.* Figs. 3, 9, and 17). Inward from the crystal tip along [010], the conversion of metatamboite to tamboite is complete over a distance of perhaps 100 μm or more. The $\{H_2O\}_4$ clusters are inhibited from penetrating deeper into the crystal and the conversion to tamboite is incomplete. This incomplete metatamboite → tamboite transition along the length of the crystal-fiber composite couples to differential shear along $[20\bar{1}]$, which results in the twisted fibers seen in Figure 3. As our single-crystal X-ray experiments only captured X-ray diffraction from the crystal tip, we were able to measure diffraction from small crystal volumes corresponding to 100% tamboite

Downloaded from https://pubs.geoscienceworld.org/canmin/article-pdf/57/5/605/4851376/i1499-1276-57-5-605.pdf
by University of Arizona user

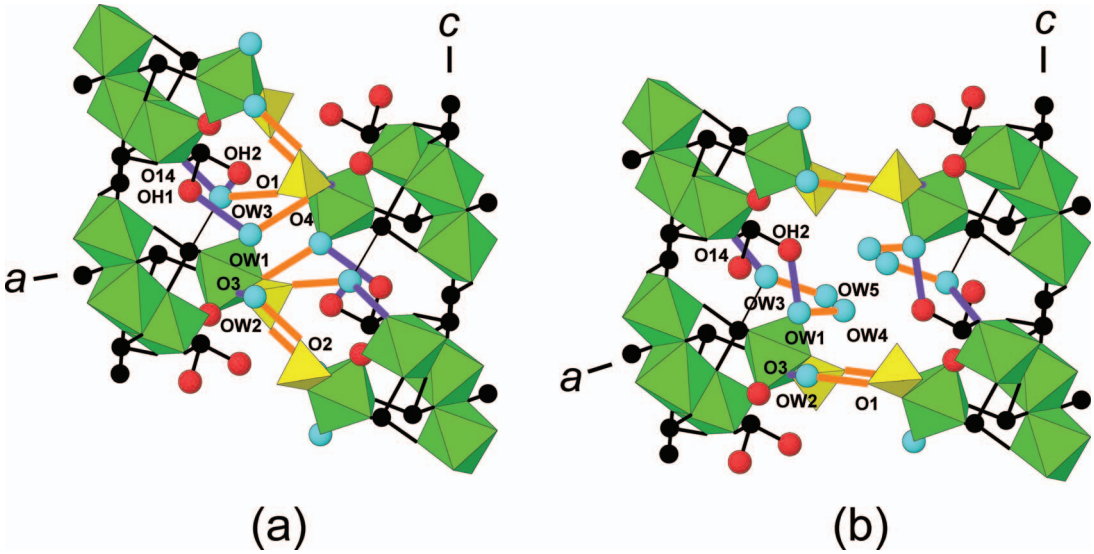

FIG. 13. The composite intra-slab hydrogen bonds (thick purple lines) and inter-slab hydrogen bonds (thick orange lines) involving the H_2O groups bonded to cations in (a) metatamboite, (b) tamboite, projected down [010].

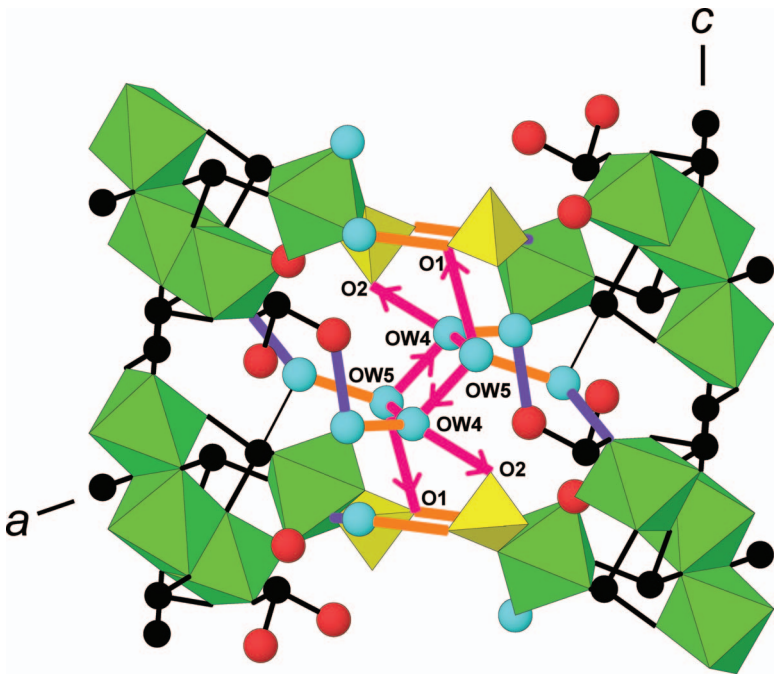

FIG. 14. The inter-slab hydrogen bonds (thick fuschia lines) donated by the interstitial {H_2O} groups OW(4) and OW(5) in tamboite, projected down [010]. Legend as in Figure 13.

Downloaded from https://pubs.geoscienceworld.org/canmin/article-pdf/57/5/605/4851376/i1499-1276-57-5-605.pdf
by University of Arizona user

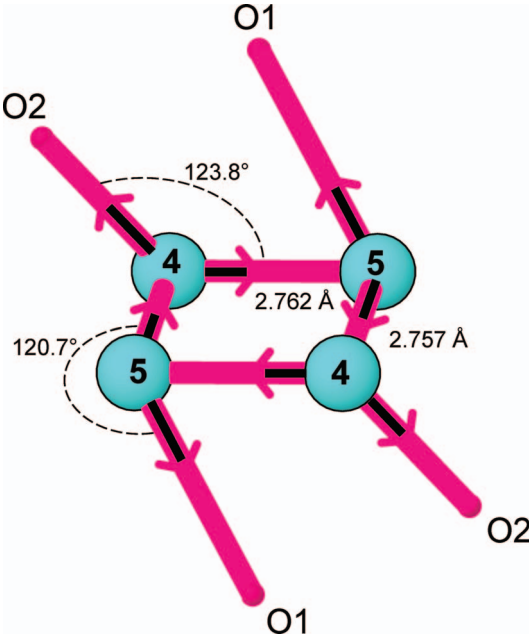

FIG. 15. An isolated $\{H_2O\}_4$ cyclic tetramer in tamboite.

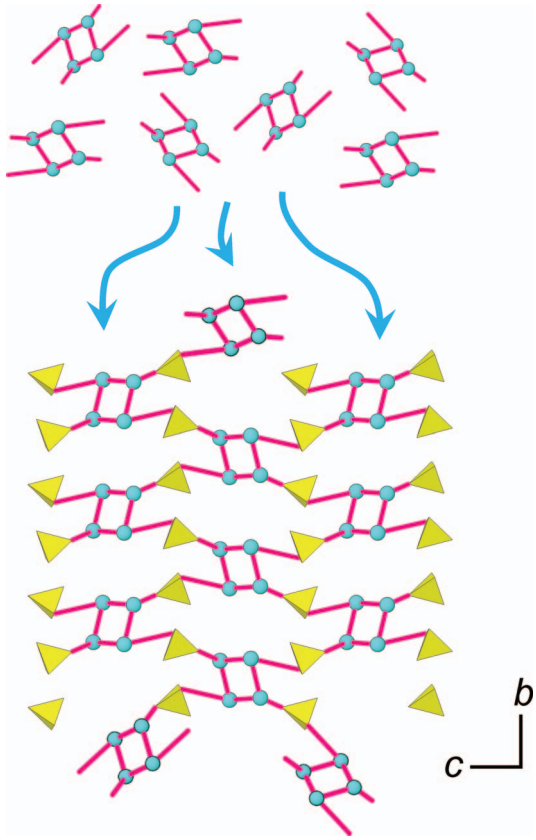

FIG. 16. A depiction of atmospheric $\{H_2O\}_4$ water clusters entering or exiting the interstitial region along [010], projected onto (100).

or 100% metatamboite at different relative humidities in the zone of complete conversion; the consistency of the simple flat prismatic habit at the tip may be considered visual confirmation of complete transition.

THE CRYSTAL STRUCTURE OF THE LOWER HYDRATE [LH]

LH X-ray data collection and refinement

The original X-ray crystal (crystal #1) that produced the metatamboite structure in winter and the tamboite unit-cell the following summer was sealed in a low-humidity environment at room temperature for approximately six months and subsequently gave a distinctly different unit-cell the following winter (Table 3). This new unit-cell was verified at the beginning and end of the X-ray data collection, indicating that the crystal remained stable while exposed to the lower humidity in the lab during X-ray data acquisition. There are two important visual characteristics of the LH crystal that differ from those of tamboite and metatamboite: (1) the LH crystal is a darker honey-brown color, and (2) the tip of the LH crystal has a pronounced curvature along (100) (Fig. 5). Given the flexure of the crystal tip, it is not surprising that the X-ray diffraction maxima show significant streaking. Several data runs oriented less favorably with respect to the streaking direction failed to produce stable frame-integration results, and these data runs were excluded from the final merged intensities. Of the 17,673 reflections successfully integrated, 7875 individual Ewald reflections remained after merging of identical reflections following absorption correction. The merging of identical reflections gave an internal agreement index of 28.5%, clearly indicating the poorer quality of the diffraction data from this bent crystal. For $P2_1/c$ symmetry, there are 2118 unique reflections with an $R_{merge} = 31.5\%$, which is poor but in accord with the internal-agreement index. The systematically absent reflections and E statistics are consistent with $P2_1/c$ symmetry, and a structure related to tamboite/metatamboite was solved in this space group. We were able to refine a fully convergent structure model with reasonable independent isotropic-displacement parameters for the cations and a mutually dependent isotropic-displacement parameter for the anions; the isotropic-displacement parameter of the more loosely bonded OW(3) anion was allowed to refine indepen-

Downloaded from https://pubs.geoscienceworld.org/canmin/article-pdf/57/5/605/4851376/i1499-1276-57-5-605.pdf
by University of Arizona user

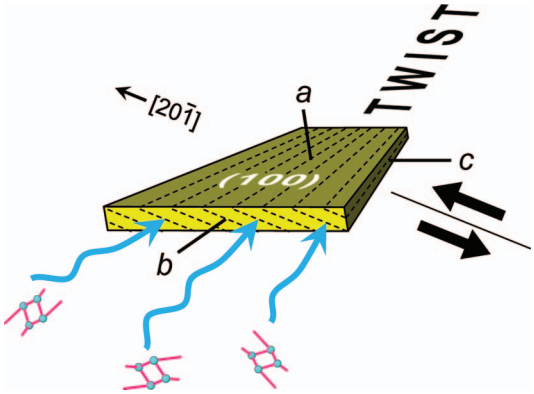

FIG. 17. Perspective view of atmospheric $\{H_2O\}_4$ water clusters entering the crystal tip along [010]. Dashed lines mark (201) shear planes along which sinistral movement between structural slabs occurs along [20$\bar{1}$].

dently. The final R_1 of 25.4% would normally not be considered acceptable. However, given the bent nature of the crystal, we were amazed that we could get diffraction from the crystal at all, let alone obtain an interpretable structure solution. The overall connectivity (coordination environments and bond lengths) for the LH structure are strikingly similar to those of the more precisely determined tamboite and metatamboite structures. The standard deviations of the interatomic distances in the LH structure are an order of magnitude greater than those in tamboite/metatamboite structures (Tables 4 and 5), preventing comparison of bond lengths and associated bond-valences for the structures. Nevertheless, using the tamboite and metatamboite structures as a guide, along with the above-mentioned geometric criteria pertaining to feasible O_D–O_A relations, we were able to derive a reasonable hydrogen-bond assignment for the LH structure (Table 9).

The chemical formula of the lower-hydrate [LH] structure

The majority of the LH structure strongly resembles that of tamboite/metatamboite and here we focus only on the important differences. The atom positions in the asymmetric unit and atom labels for all three structures have been maintained in an absolute sense to facilitate comparison. In tamboite and metatamboite, the O(1) anion belonging to the (SO_4) group is interpreted as an (OH) group in the LH structure; thus the LH structure has no O(1) atom, and instead the OH(4) label is used for the analogous SO_4 vertex. In the LH structure, the O(2) anion belonging to the (SO_4) group is also bonded to Fe(2). The Fe(2) atom is octahedrally coordinated in all three

TABLE 9. PROPOSED HYDROGEN BONDING* FOR THE LOWER HYDRATE (LH)

OH(1)···OW(3)	3.39(12)
OH(2)···O(4)	2.91(8)
OH(3)···O(3)	2.80(10)
OH(4)···OW(3)	3.36(12)
OW(1)···OH(4)	2.90(11)
OW(1)···OH(2)	2.90(10)
OH(4)–OW(1)–OH(2)	121(3)
OW(3)···OH(4)	2.96(8)
OW(3)···O(14)	2.75(11)
OH(4)–OW(3)–O(14)	110(3)

* Distances (Å), angles (°).

structures. However, the OW(2) anion (in tamboite and metatamboite) has been replaced by the O(2) anion in the LH structure; thus the (H_2O) group that coordinates Fe(2) in tamboite and metatamboite has been removed from the LH structure, and the (SO_4) group moves closer to Fe(2) to share its O(2) anion with the Fe(2) atom. The anions O(2)–O(14), OH(1)–OH(3), OW(1), and OW(3) are identical in all three structures. The other anion sites have the following identities in the three structures: $O(1)_{TAM,MTAM} = OH(4)_{LH}$, $OW(2)_{TAM,MTAM} = O(2)_{LH}$, and $OW(4,5)_{TAM} = \square_{MTAM,LH}$. The removal of a cation-bonded (H_2O) group from the OW(2) site in tamboite and metatamboite is very significant from a structural perspective, although its absence in the LH structure does not affect electroneutrality. However, the replacement of O^{2-} at the O(1) site in tamboite and metatamboite with an $(OH)^-$ group in the LH structure requires an accompanying charge-balance mechanism. We consider reduction of some of the Fe from Fe^{3+} to Fe^{2+} to be the most feasible process to maintain charge balance, and this is discussed in more detail in the subsequent section. The chemical formula for the LH crystal developed from the structural interpretation is $Fe^{3+}{}_2Fe^{2+}(SO_3(OH))(Te^{4+}O_3)_3(Te^{4+}O(OH)_2)(OH)(H_2O)_2$; like metatamboite, the LH structure has no interstitial $\{H_2O\}$. However, the desiccating environment to which the LH crystal was exposed has resulted in (1) removal of a bonded (H_2O) group, (2) protonation of the (SO_4) group, and (3) partial reduction of Fe^{3+}. We were unable to reverse these changes *via* attempted rehydration of the LH crystal, either passively in the higher humidity of summer, or by isolation in a near-saturated sealed test-tube at room temperature.

Downloaded from https://pubs.geoscienceworld.org/canmin/article-pdf/57/5/605/4851376/i1499-1276-57-5-605.pdf
by University of Arizona user

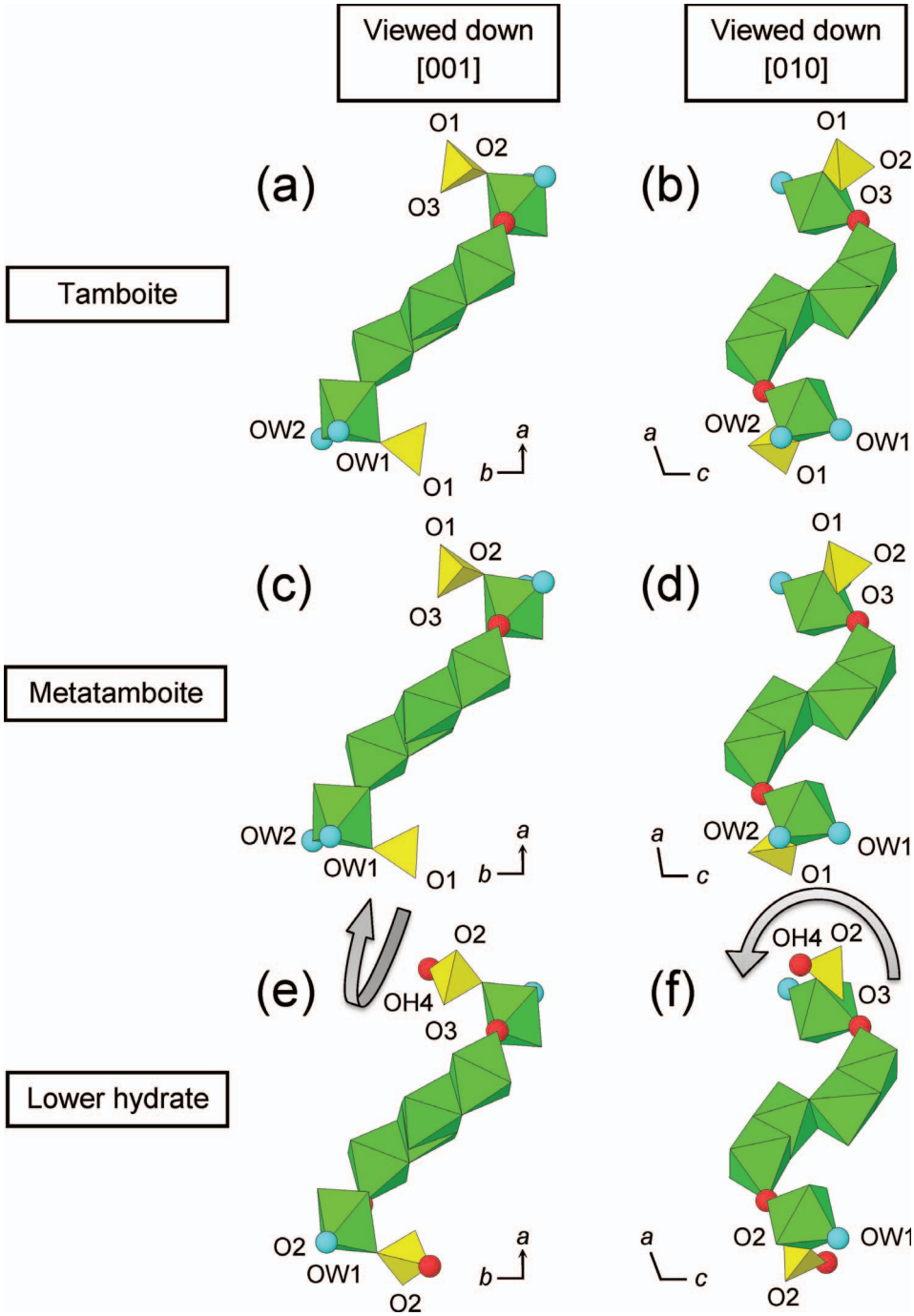

FIG. 18. The ferric-sulfate-hydrate strand oriented down [001] and [010] in (a and b) tamboite; (c and d) metatamboite; (e and f) lower hydrate. Curved hollow arrows indicate the rotation direction of ($S\Phi_4$) groups in LH relative to tamboite/metatamboite.

Downloaded from https://pubs.geoscienceworld.org/canmin/article-pdf/57/5/605/4851376/i1499-1276-57-5-605.pdf
by University of Arizona user

Identification of the $SO_3(OH)$ group and Fe^{2+} in the LH structure

In all three structures, the $O(1)_{TAM,MTAM}$ or $OH(4)_{LH}$ anion of the ($S\Phi_4$) group receives all of its bond valence from a combination of S^{6+} and H^+. In the LH structure, this particular anion is much further from the *S* site than in the tamboite and metatamboite structures (1.64 *versus* 1.453 and 1.422 Å, Table 5) and receives a substantially lower bond-valence from the S^{6+} ion (*i.e.*, ~1 *vu*). If the $OH(4)_{LH}$ anion were O^{2-}, it would have to accept at least three (or more) strong hydrogen bonds in order to satisfy the valence-sum rule. However, there are no neighboring $(OH)^-$ or (H_2O) groups in the LH structure that can donate strong hydrogen bonds to this anion. Thus, the long S–OH(4) bond, in combination with the lack of strong incident hydrogen bonds, requires that OH(4) must be an (OH) group and not an O^{2-} ion. In the dehydration process, the conversion of an O^{2-} ion to an $(OH)^-$ group requires an accompanying redox change in the crystal in order to maintain electroneutrality. This change may involve either another change in anion identity [*i.e.*, $(OH)^- \rightarrow O^{2-}$ or $(H_2O) \rightarrow (OH)^-$] or a change in cation identity (*i.e.*, $Fe^{3+} \rightarrow Fe^{2+}$). The only other substantial difference (relative to tamboite and metatamboite) in the environment of an anion is in relation to the polymerization of the ferric-sulfate-hydrate strands *via* S–O(2)–Fe(2) bridges in the LH structure; however, this difference in connectivity does not involve any change in anion charge, as the O(2) anion is O^{2-} before and after the transformation. The large standard deviation of the observed bond lengths in the LH structure (Table 5) does not allow assessment of any change in ionic radius of the constituent cations. However, Fe octahedra share edges [O(10)–O(13) for Fe(1)–Fe(1) and O(7)–O(7)′ for Fe(1)–Fe(2)] within the central region of the ferric-sulfate-hydrate strand (Fig. 7), allowing IVCT (inter-valence charge-transfer) between Fe^{3+} and Fe^{2+} at these sites. The LH crystal is a darker honey-brown color than is tamboite or metatamboite, suggesting the occurrence of both Fe^{3+} and Fe^{2+} at the *Fe* sites. Thus, partial reduction of Fe^{3+} to Fe^{2+} seems the most likely mechanism to charge-balance the presence of the $SO_3(OH)$ group in the LH structure.

Bond topology of the lower hydrate LH structure

The core structural component in all three structures is the ferric-sulfate-hydrate strand. This part of the LH structure contains two differences in the type of anion relative to the structures of tamboite and metatamboite: $O(1)_{TAM,MTAM} = OH(4)_{LH}$, and $OW(2)_{TAM,MTAM} = O(2)_{LH}$. However, the overall bond-topology of an isolated strand remains the same (Fig. 18). The most significant geometric difference within the strands between the LH structure and the tamboite and metatamboite structures relates to the position of the $SO_3(OH)$ group. In tamboite and metatamboite, the (SO_4) group has the O(1) anion at the end of the strand along **a*** (Fig. 18a, b, c, and d), whereas in the LH structure, the $SO_3(OH)$ group is rotated relative to its position in tamboite and metatamboite, such that the O(2) anion now lies at the extreme end of the strand (Fig. 18e and f). Also in the ferric-sulfate-hydrate strand in the LH structure (Fig. 18e and f), the O(2) is attached to the Fe(3) octahedron in place of the (H_2O) group $[OW(2)]_{TAM,MTAM}$ (Fig. 18a, b, c, and d).

In metatamboite, adjacent structural slabs are separated by a narrow gap that is bridged by hydrogen bonds (Figs. 9a and 13a). The inter-slab hydrogen bond from OW(2) to O(2) in metatamboite has an OW(2)···O(2) distance of 2.68 Å (Fig. 13a, Table 8). The fusion of adjacent strands in the LH structure is best viewed along [102], where adjacent OW(2) and O(2) sites in metatamboite (Fig. 19a) merge to form the single O(2) site in the LH structure (Fig. 19b). This merging is facilitated by rotation of the $SO_3(OH)$ tetrahedron in the LH structure where the O(2) vertex is turned toward the adjacent strand. As in the metatamboite → tamboite transition (Fig. 9), we can understand the metatamboite → LH transition by examining the relative displacement of adjacent structural slabs, viewed along [010] in Figure 20. In the LH structure, the direct linkage of slabs across the interstitial gap at $x = ½$ in metatamboite (Fig. 20a) occurs primarily *via* a ~2.5 Å left-lateral displacement along $[00\bar{1}]$, which is consistent with the small difference in unit-cell lengths between metatamboite and LH and the 12.3° increase in β angle for the LH structure (Table 3). As was the case for incomplete tamboite ↔ metatamboite conversion, a similar incomplete metatamboite → LH conversion is likely to couple with shear between adjacent slabs [in this case, along the (100) plane]. We regard the visual curvature of the LH crystal along (100) as macroscopic evidence of this process (*cf.* Figs. 4 and 20b). The linkage of structural slabs in the LH crystal (Fig. 20b) changes the general classification of the structure: the ferric-sulfate-hydrate slabs that characterize the sheet character of the tamboite/metatamboite structures have polymerized to form a framework structure in the LH crystal.

At ½,*y*,½ in the unit cell of LH, there is a rather constricted empty channel lined with (OH) and (H_2O) groups (central region of Fig. 20b). Hydrogen bonding propagates around this channel (Fig. 21a), but the restricted channel dimensions do not allow internal occupancy by an {H_2O} group, and no residual

Downloaded from https://pubs.geoscienceworld.org/canmin/article-pdf/57/5/605/4851376/i1499-1276-57-5-605.pdf
by University of Arizona user

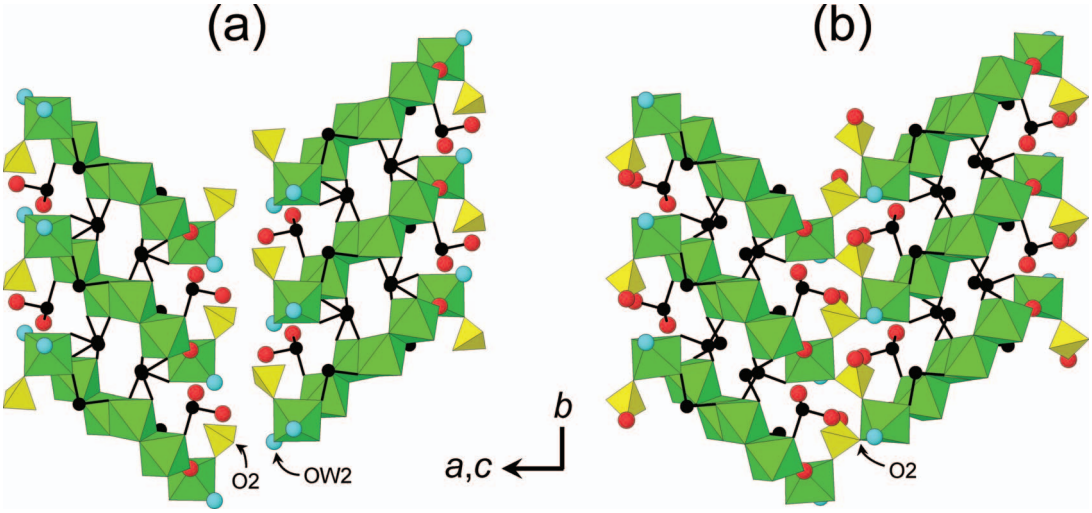

FIG. 19. Connectivity between ferric-sulfate-hydrate columns in (a) metatamboite, (b) lower hydrate; projected onto $(10\bar{2})$.

electron-density was found in difference-Fourier maps along its central axis. A hydrogen-bonding arrangement for the LH structure is given in Table 9 and illustrated edge-on for a single channel in Figure 21b. The O(2) anion of the (SO_4) group that accepts multiple hydrogen bonds in the tamboite/metatamboite structure (*i.e.*, three hydrogen bonds summing to 0.45 *vu*) does not accept any hydrogen bonds in the LH structure; the O(2) anion is now bonded to Fe^{3+} at the *Fe*(3) site. In the tamboite/metatamboite structure, the O(3) anion of the (SO_4) group accepts a strong interslab hydrogen bond from the (H_2O) group at OW(2) and a weak bifurcated hydrogen bond from a neighboring OH(3). In the transition from tamboite/

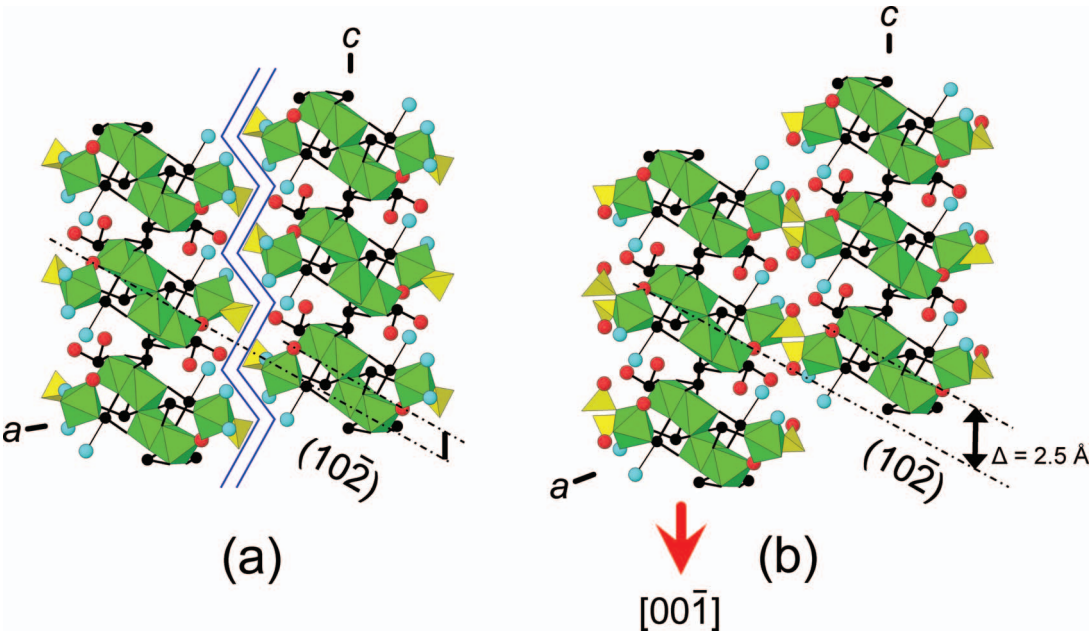

FIG. 20. Adjacent (100) structural slabs viewed down [010] in (a) metatamboite, (b) lower hydrate (fused). Legend as in Figure 9.

Downloaded from https://pubs.geoscienceworld.org/canmin/article-pdf/57/5/605/4851376/i1499-1276-57-5-605.pdf
by University of Arizona user

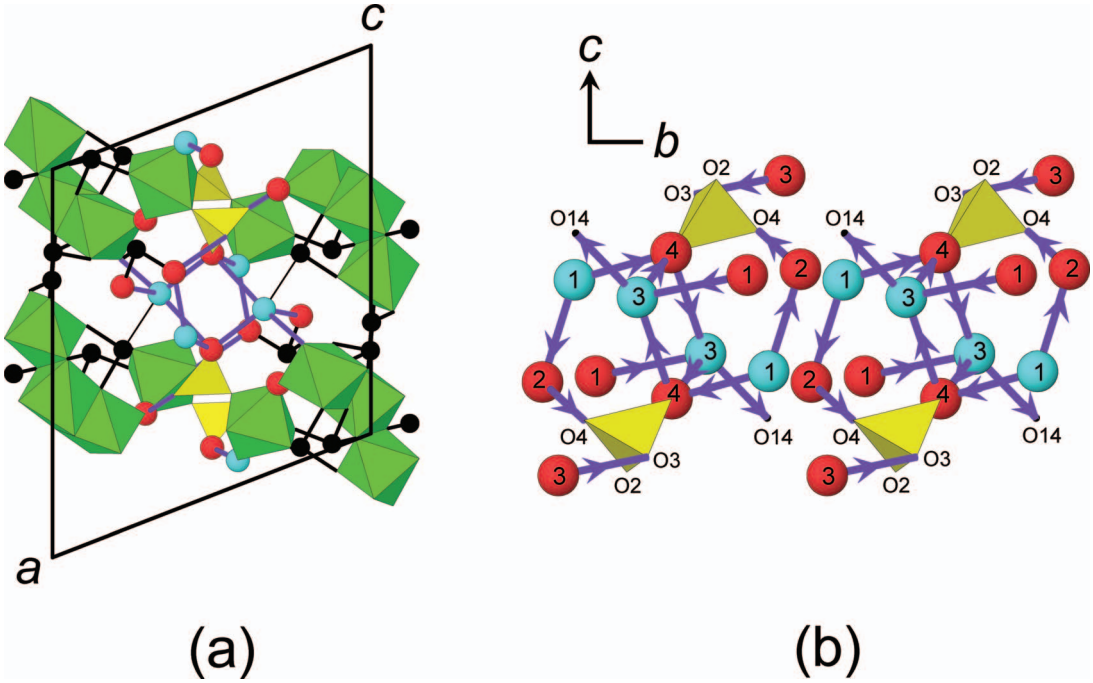

FIG. 21. The hydrogen bonding associated with the (OH) groups (red circles) and (H_2O) groups (blue circles) in the LH structure: (a) projected down [010]; (b) projected down an axis slightly rotated from [100].

metatamboite to the LH structure, the (SO_4) group rotates to bring its O^{2-} ion at the O(3) site closer to the $(OH)^-$ ion at the OH(3) site and the O^{2-} ion at O(3) accepts a single strong hydrogen bond from this $(OH)^-$ group at OH(3). The OH(4) anion of the $SO_3(OH)$ tetrahedron in the LH structure now has an attached H^+ ion, forming an $(OH)^-$ group, and also receives two weak hydrogen bonds, one from the (H_2O) group at OW(1) and one from the (H_2O) group at OW(3) (Table 9). The net bond-valence incident at the OH(4) anion is thus 1.00 *vu* (from S^{6+}) + 0.90 (from the associated H^+ ion) + 0.10 [from $OW(1)_D$] + 0.05 [from $OW(3)_D$] = 2.05 *vu*, which supports the assignment of OH to the OH(4) site in the LH structure. The remaining anion of the $SO_3(OH)$ tetrahedron is O^{2-} at O(4) that is also bonded to Fe(3). As in metatamboite, the O(4) anion in the LH structure receives a single weak hydrogen bond, but it is donated from OH(2) in the LH structure and from OW(1) in metatamboite. As a result of the relative displacement between structural slabs and rearrangement of possible O_A anions, the hydrogen bonds associated with the (H_2O) group at OW(1) differs in the LH structure, with anions at OH(2) and OH(4) as acceptors (Table 9, Fig. 21). The hydrogen bonds associated with OW(3) are the same in both metatamboite and LH: one hydrogen-bond is donated to O(14) and the other is donated to $O(1)_{MTAM}$ or $OH(4)_{LH}$ (Figs. 13a and 21).

CONCLUSIONS

The discovery of tamboite and metatamboite, and their sensitivity to ambient humidity, has allowed us to examine the mechanism of hydration-dehydration in a complicated crystal structure. Of particular interest is the identification of the C_i cyclic tetramer $\{H_2O\}_4$ as the principal mobile component in the hydration-dehydration process. This tetramer is a major constituent of the Earth's lower-atmosphere under humid conditions, and it is tempting to relate the hydration of metatamboite to form tamboite directly to the increased activity of the C_i cyclic tetramer in the atmosphere at higher humidity. Thus, we have presented the tamboite-metatamboite hydration-dehydration reaction as involving uptake (tamboite) or release (metatamboite) of the *Ci* cyclic tetramer $\{H_2O\}_4$. This mechanism is based on similar geometries and homodromic hydrogen-bonding characteristics shared between the structurally bound $\{H_2O\}_4$ clusters in tamboite and those found in humid atmosphere. We have no way of knowing directly if *Ci* cyclic tetramers $\{H_2O\}_4$ were absorbed intact into the metatamboite structure to produce tamboite, or if

Downloaded from https://pubs.geoscienceworld.org/canmin/article-pdf/57/5/605/4851376/i1499-1276-57-5-605.pdf
by University of Arizona user

isolated (H_2O) groups entered the structure and combined within the structure to form the observed *Ci* cyclic tetramers $\{H_2O\}_4$. Other small $\{H_2O\}$ clusters are stable constituents of the atmosphere and can potentially engage in the hydration-dehydration of minerals. Presumably the details of the local atom arrangements around the absorbed clusters will dictate the type of cluster active in specific mineral reactions, and it is of considerable interest to identify which other atmospheric $\{H_2O\}$ clusters may be active in such hydration-dehydration reactions.

Acknowledgments

We appreciate the comments of two anonymous reviewers. This work was supported by a Discovery grant from the Natural Sciences and Engineering Research Council of Canada, and by grants from the Canada Foundation for Innovation, both to FCH.

References

Back, M.E., Grice, J.D., Gault, R.A., Criddle, A.J., & Mandarino, J.A. (1999) Walfordite, a new tellurite species from the Wendy open pit, El Indio-Tambo mining property, Chile. *Canadian Mineralogist* **37**, 1261–1268.

Back, M.E., Grice, J.D., Cooper, M.A., Gault, R.A., Walford, P.C., & Mandarino, J.A. (2017) Telluromandarinoite, a new tellurite mineral from the El Indio-Tambo mining property, Andes Mountains, Chile. *Canadian Mineralogist* **55**, 21–28.

Burns, P.C., Cooper, M.A., & Hawthorne, F.C. (1995) Parakhinite, $Cu^{2+}{}_3PbTe^{+6}O_6(OH)_2$: crystal structure and revision of chemical formula. *Canadian Mineralogist* **33**, 33–40.

Christy, A.G., Kampf, A.R., Mills, S.J., Housley, R.M., & Thorne, B. (2015) Crystal structure and revised chemical formula for burckhardtite, $Pb_2(Fe^{3+}Te^{6+})[AlSi_3O_8]O_6$: a double-sheet silicate with intercalated phyllotellurate layers. *Mineralogical Magazine* **78**, 1763–1773.

Christy, A.G., Mills, S.J., & Kampf, A.R. (2016a) A review of the structural architecture of tellurium oxycompounds. *Mineralogical Magazine* **80**, 415–545.

Christy, A.G., Mills, S.J., Kampf, A.R., Housley, R.M., Thorne, B., & Marty, J. (2016b) The relationship between mineral composition, crystal structure and paragenetic sequence: the case of secondary Te mineralization at the Bird Nest drift, Otto Mountain, California, USA. *Mineralogical Magazine* **80**, 291–310.

Cooper, M.A. & Hawthorne, F.C. (1996) The crystal structure of spiroffite. *Canadian Mineralogist* **34**, 821–826.

Cooper, M.A., Hawthorne, F.C., & Back, M. (2008) The crystal structure of khinite and polytypism in khinite and parakhinite. *Mineralogical Magazine* **72**, 763–770.

Day, M.B., Kirschner, K.N., & Shields, G.C. (2005) Global search for minimum energy $(H_2O)_n$ clusters, $n = 3 - 5$. *Journal of Physical Chemistry* **A109**, 6773–6778.

Dunn, M.E., Pokon, E.K., & Shields, G.C. (2004) The ability of the Gaussian-2, Gaussian-3, Complete Basis Set–QB3, and Complete Basis Set–APNO model chemistries to model the geometries of small water clusters. *International Journal of Quantum Chemistry* **100**, 1065–1070.

Gagné, O.C. & Hawthorne, F.C. (2015) Comprehensive derivation of bond-valence parameters for ion pairs involving oxygen. *Acta Crystallographica* **B71**, 562–578.

Gagné, O.C. & Hawthorne, F.C. (2018a) Bond-length distributions for ions bonded to oxygen: Metalloids and post-transition metals. *Acta Crystallographica* **B74**, 63–78.

Gagné, O.C. & Hawthorne, F.C. (2018b) Bond-length distributions for ions bonded to oxygen: Results for the non-metals and discussion of lone-pair stereoactivity and the polymerization of PO_4. *Acta Crystallographica* **B74**, 79–96.

Hawthorne, F.C. (1984) The crystal structure of mandarinoite, $Fe^{3+}{}_2Se_3O_9.6H_2O$. *Canadian Mineralogist* **22**, 475–480.

Hawthorne, F.C. (1992) The role of OH and H_2O in oxide and oxysalt minerals. *Zeitschrift für Kristallographie* **201**, 183–206.

Hawthorne, F.C. (2015) Generating functions for stoichiometry and structure of single- and double-layer sheet-silicates. *Mineralogical Magazine* **79**, 1675–1709.

Hawthorne, F.C., Ercit, T.S., & Groat, L.A. (1986) The structure of zinc selenite and copper selenite. *Acta Crystallographica* **C42**, 1285–1287.

Hawthorne, F.C., Groat, L.A., & Ercit, T.S. (1987) Structure of cobalt diselenite. *Acta Crystallographica* **C43**, 2042–2044.

Hawthorne, F.C., Krivovichev, S.V., & Burns, P.C. (2000) The crystal chemistry of sulfate minerals. *In* Sulfate Minerals: Crystallography, Geochemistry and Environmental Significance (C.N. Alpers, J.L. Jambor, & D.K. Nordstrom, eds.). Mineralogical Society of America, Washington, D.C., *Reviews in Mineralogy and Geochemistry* **40**, 1–112.

Hawthorne, F.C., Cooper, M.A., & Back, M.E. (2009) Khinite-4*O* [= khinite] and khinite-3*T* [= parakhinite]. *Canadian Mineralogist* **47**, 473–476.

Kampf, A.R., Housley, R.M., Mills, S.J., Marty, J., & Thorne, B. (2010) Lead-tellurium oxysalts from Otto Mountain near Baker, California: I. Ottoite, Pb_2TeO_5, a new mineral with chains of tellurate octahedra. *American Mineralogist* **95**, 1329–1336.

Kampf, A.R., Mills, S.J., Housley, R.M., & Marty, J. (2013a) Lead-tellurium oxysalts from Otto Mountain near Baker,

Downloaded from https://pubs.geoscienceworld.org/canmin/article-pdf/57/5/605/4851376/i1499-1276-57-5-605.pdf
by University of Arizona user

California: VIII. Fuettererite, $Pb_3Cu^{2+}{}_6Te^{6+}O_6(OH)_7Cl_5$, a new mineral with double spangolite-type sheets. *American Mineralogist* **98**, 506–511.

Kampf, A.R., Mills, S.J., Housley, R.M., & Marty, J. (2013b) Lead-tellurium oxysalts from Otto Mountain near Baker, California: IX. Agaite, $Pb_3Cu^{2+}Te^{6+}O_5(OH)_2(CO_3)$, a new mineral with CuO_5–TeO_6 polyhedral sheets. *American Mineralogist* **98**, 512–517.

Kampf, A.R., Cooper, M.A., Mills, S.J., Housley, R.M., & Rossman, G.R. (2016) Lead-tellurium oxysalts from Otto Mountain near Baker, California: XII. Andychristyite, $PbCu^{2+}Te^{6+}O_5(H_2O)$, a new mineral with HCP stair-step layers. *Mineralogical Magazine* **80**, 1055–1065.

Kampf, A.R., Housley, R.M., & Marty, J. (2017) Dagenaisite, a new zinc tellurate from the gold chain mine, tintic, Utah, USA. *Canadian Mineralogist* **55**, 867–873.

Kampf, A.R., Housley, R.M., Rossman, G.R., Marty, J., & Chorazewich, M. (2018) Bodieite, $Bi^{3+}{}_2(Te^{4+}O_3)_2(SO_4)$, a new mineral from the Tintic District, Utah, and the Masonic District, California, USA. *Canadian Mineralogist* **56**, 763–772.

Maheshwary, S., Patel, N., Sathyamurthy, N., Kulkarni, A.D., & Gadre, S.R. (2001) Structure and stability of water clusters $(H_2O)_n$, $n = 8$–20: an Ab Initio investigation. *Journal of Physical Chemistry* **A105**, 10525–10537.

Mills, S.J. & Christy, A.G. (2013) Revised values of the bond valence parameters for Te^{IV}–O, Te^{VI}–O and Te^{IV}–Cl. *Acta Crystallographica* **B69**, 145–149.

Mills, S.J., Kampf, A.R., Christy, A.G., Housley, R.M., Rossman, G.R., Reynolds, R.E., & Marty, J. (2014) Mojaveite and bluebellite, two new minerals from the central Mojave Desert, California, USA. *Mineralogical Magazine* **78**, 1325–1340.

Missen, O.P., Mills, S.J., Spratt, J., Welch, M.D., Birch, W.D., Rumsey, M.S., & Vylita, J. (2018) The crystal-structure determination and redefinition of eztlite, $Pb_2{}^{2+}Fe_3{}^{3+}(Te^{4+}O_3)_3(SO_4)O_2Cl$. *Mineralogical Magazine* **82**, 1355–1367.

Pouchou, J.L. & Pichoir, F. (1985) 'PAP' φ(ρZ) procedure for improved quantitative microanalysis. *In* Microbeam Analysis (J.T. Armstrong, ed.). San Francisco Press, San Francisco, California, United States (104–106).

Sheldrick, G.M. (2008) A short history of *SHELX*. *Acta Crystallographica* **A64**, 112–122.

Shields, R.M., Temelso, B., Archer, K.A., Morrell, T.E., & Shields, G.C. (2010) Accurate predictions of water cluster formation, $(H_2O)_{n=2–10}$. *Journal of Physical Chemistry* **A114**, 11725–11737.

Siddeley, G. & Araneda, R. (1986) The El Indio-Tambo gold deposits, Chile. *In* Proceedings Gold '86 (A.J. MacDonald, ed.). Konsult International, Toronto, Ontario, Canada (445–456).

Tait, K.T., DiCecco, V., Ball, N.A., Hawthorne, F.C., & Kampf, A.R. (2014) Backite, $Pb_2Al(TeO_6)Cl$, a new tellurate mineral from the Grand Central mine, Tombstone Hills, Cochise Country, Arizona: Description and crystal structure. *Canadian Mineralogist* **52**, 935–942.

Received January 9, 2019. Revised manuscript accepted June 12, 2019.

Downloaded from https://pubs.geoscienceworld.org/canmin/article-pdf/57/5/605/4851376/i1499-1276-57-5-605.pdf
by University of Arizona user